The Atmospheric Oxidizing Capacity in China: Part 2. Sensitivity to emissions of primary pollutants

Jianing Dai[a], Guy P. Brasseur[a,e,f], Mihalis Vrekoussis[b,g,h], Maria Kanakidou[b,d], Kun Qu[b], Yijuan Zhang[b], Hongliang Zhang[c], Tao Wang[f]

[a] Environmental Modelling Group, Max Planck Institute for Meteorology, Hamburg, 20146, Germany
[b] Institute of Environmental Physics (IUP), University of Bremen, Bremen, 28359, Germany
[c] Department of Environmental Science and Engineering, Fudan University, Shanghai, 200433, China
[d] Environmental Chemical Processes Laboratory, Department of Chemistry, University of Crete, Heraklion, 70013, Greece
[e] National Center for Atmospheric Research, Boulder, Colorado, 80307, USA
[f] Department of Civil and Environmental Engineering, The Hong Kong Polytechnic University, Hong Kong, China
[g] Center of Marine Environmental Sciences (MARUM), University of Bremen, Bremen, 28359, Germany
[h] Climate and Atmosphere Research Center (CARE-C), The Cyprus Institute, Nicosia, Cyprus

Correspondence to: Guy P. Brasseur (guy.brasseur@mpimet.mpg.de)

Abstract

Despite substantial reductions in anthropogenic emissions, ozone (O_3) pollution remains a severe environmental problem in urban China. These reductions affect ozone formation by altering the levels of O_3 precursors, intermediates, and the oxidation capacity of the atmosphere. However, the underlying mechanisms driving O_3 changes are still not fully understood. Here, we employ a regional chemical transport model to quantify the ozone changes due to a specified emission reduction (50%) for winter and summer conditions of 2018. Our results indicate that reduction in nitrogen oxide (NO_x) emissions increase surface O_3 concentrations by 15%−33% on average across China in winter and by up to 17% in the volatile organic compounds (VOCs)-limited areas during summer. These ozone increases are associated with a reduced NO_x-titration effect and higher levels of OH radical. Reducing the NO_x emission significantly decreases the concentration of particulate nitrate, which enhances ozone formation through increased HO_2 radical levels due to reduced aerosol uptake and diminished aerosol extinction. Additionally, an enhanced atmospheric oxidative capacity, driven by larger contributions from the photolysis of OVOCs and OH-related reactions, also favors urban ozone formation. With additional reductions in anthropogenic VOCs emissions, increases in summertime ozone (VOC-limited areas) can be offset by the reduced production of radicals from VOCs oxidations. To effectively mitigate ozone pollution, a simultaneous reduction in the emission of NO_x and specific VOCs species should be applied, especially regarding alkenes, aromatics, and unsaturated OVOCs, including methanol and ethanol.

Keywords: ozone pollution, emission reduction, WRF-Chem, *AOC*

1. Introduction

To effectively reduce air pollution in China, the government of the country has implemented stringent actions between 2013 and 2020 (Liu et al., 2020; Liu et al., 2023). In the initial phase, from 2013 to 2017, the control of primary pollutants was particularly effective, with a dramatic decrease in the anthropogenic emissions of fine particles ($PM_{2.5}$), sulfur dioxide (SO_2), and nitrogen oxides (NO_x) (Zheng et al., 2018; Liu et al., 2020). In subsequent years, a sustained reduction in the emission of SO_2, NO_x, and $PM_{2.5}$ was achieved, particularly between 2018 and 2020 (Liu et al., 2023). The implementation of the emission control policies has greatly improved China's air quality. However, a significant increase in the surface ozone (O_3) concentration was observed from 2013 to 2019, with the positive trend slowing down in 2020 and 2021, but rebounding in 2022 (Liu et al., 2023; China Air 2023). Several studies provide explanations for the positive trend observed in the surface O_3 concentration, including a reduction in the NO_x emissions and in the atmospheric aerosol load (Li et al., 2019; Liu et al., 2020). During and after the recent COVID-19 lockdown period, ozone pollution has been reported to happen, which is believed to be favored by a sharp reduction of NO_x and high emissions of volatile organic compounds (VOCs) (Li et al., 2021). Looking through these changes over the past decade, we learn that rapid reductions of emissions disturb substantially ozone chemistry and, thereby, produce changes in the ozone concentrations.

The response of ozone to reduced NO_x emissions varies with the local photochemical environment and specifically with the encountered chemical regimes (i.e., VOC-limited, NO_x-limited, or transition conditions) (Jacob., et al., 1995; Ou et al., 2016; Dai et al., 2023). In NO_x-sensitive regimes, the reduction in NO_x emissions decreases the number of NO_2 molecules photolyzed, leading to fewer ozone molecules being produced. While, in VOC-sensitive regimes, the reduction in the NO_x abundance tends to enhance the ozone formation due to the weakening of NO titration and to the reduced loss of OH radical by the reaction with NO_2. Several studies based on satellite observations (Wang et al., 2021) and regional models (Zhu et al., 2023) have shown that the reduction in anthropogenic emissions has generated a change in the geographical distribution of the ozone formation regimes in China. These studies have reported a shift of ozone sensitivity regimes from VOC-sensitive to transition and/or even to NO_x-sensitive regimes in many metropolitan and suburban regions of East China. The shift towards NO_x-limited conditions facilitates the implementation of an efficient ozone control

through the reduction in NO_x emissions only. In the remaining VOC-sensitive and transition areas, NO_x emission reduction fails to effectively mitigate ozone pollution. In this situation, a coordinated reduction in anthropogenic VOCs (AVOCs) emissions should be implemented to effectively limit the ozone formation (Liu et al., 2023; Zhu et al., 2023). The source of NO_x in VOC-sensitive areas is mainly from fossil fuel combustion, while the emissions of AVOCs emissions result from a broad range of industrial, transportation and residential sources (B. Li et al., 2021; C. Li et al., 2022). To establish a cost-effective control over AVOCs emissions, the contribution of different VOCs categories to ozone formation should be accurately quantified for different areas of China.

The effect of aerosols on the O_3 formation has been considered in several modeling studies (Li et al., 2019; Liu et al., 2020). However, the influences of aerosol on the ozone production are complex due to the different effects that must be taken into consideration. (Tan et al., 2022; Dai et al., 2023). Understanding the changes in aerosol effects on the O_3 formation, when the primary emissions are further reduced, remains a necessity for implementing successful air quality control policies.

Recent observational studies combined with a source apportionment approach using observation-based models have highlighted the role of anthropogenic VOCs species, including the alkenes, aromatics, and oxidized volatile organic compounds (OVOCs), for mitigating summertime ozone formation in the urban areas in China (C. Li et al., 2022; W. Wang et al., 2022). The notable contributions of OVOCs to the oxidizing capacity of the atmosphere (*AOC*) as well as the formation of secondary organic aerosols (SOA) have been a concern in the regions of Yangzi River Delta (YRD) (J. Li et al., 2022) and Pearl River Delta (PRD) (W. Wang et al., 2022). The important role of biogenic VOCs (BVOCs) has also been highlighted in vegetated rural and urban regions in China where the oxidation of BVOCs can significantly contribute to the formation of ozone and aerosols, specifically in the PRD region (J. Wang et al., 2023; Zhang et al., 2023). However, a comprehensive evaluation of the changes in the contribution of different VOCs categories to *AOC* and in ozone chemistry in response to emission changes in different regions of China is still needed. Considering the necessity of implementing coordinated actions in several large geographical areas to further alleviate air pollution in China, regional chemical transport models are appropriate tools to assess the quantitative response of secondary pollutants and of the oxidizing capacity of the atmosphere to emission changes.

In the companion paper (Part 1; Dai et al., 2023), we use a regional chemical-meteorological model to quantify the relative contribution of different photochemical processes to the formation and destruction of near-surface photochemical radicals and ozone in different chemical environments in China. In Part 2 of the study, with the evaluated model, we assess the response of the photo-oxidative species and related parameters to an imposed reduction of primary emissions. This paper is structured as follows. Section 2 introduces the setup of the model system and describes the simulations performed for specified reduction scenarios in the emissions of primary pollutants. In Section 3, we analyze the response of near-surface concentration of ozone to the specified emission reductions. Further, we determine the drivers responsible for the resulting ozone changes; these include changes in the concentrations of ozone precursors, of the intermediates including the oxidized VOCs (OVOCs) and in the level of secondary aerosols. We also discuss the changes to be expected in the ozone formation regimes. Finally, we describe the sensitivity of the atmospheric oxidative capacity (*AOC*) to the reduction in the emissions. A summary and implication for policy making of our study is provided in Sec. 4.

2. Method

2.1. Model setting

We use the WRF-Chem model version 4.1.2 (Skamarock et al., 2019), coupled with the gas-phase chemistry mechanism MOZART (Emmons et al., 2010) and the aerosol module MOSAIC (Zaveri et al., 2008), to simulate the meteorological fields as well as the transport, the chemical and physical transformations of trace gases and aerosols. The months of January and July of 2018 are selected as representative months to conduct the simulations and to investigate the changes in secondary pollution and in the *AOC* in response to emission reductions during winter and summer, respectively. Compared to the standard version of the chemical mechanism, several updates of heterogeneous uptake on the surface of the ambient aerosol were implemented (Dai et al., 2023). As for the SOA formation, the main pathways result from the gas-phase oxidation of VOCs by atmospheric oxidants (OH, O_3, and NO_3) and from the heterogeneous formation of glyoxal SOA over the ambient aerosol (Knote et al., 2014). The model domain covers the whole geographical area of China. Analyses of modeling results at four urban sites (Beijing, Shanghai, Guangzhou, and Chengdu) are also performed.

More detailed information on the model configuration, the model validation, and the sites selected for our analysis can be found in Part 1 of our paper Dai et al., (2023).

We adopt the Multi-resolution Emission Inventory (MEIC v1.3; http://www.meicmodel.org/) to represent anthropogenic emissions in China and the CAMS-GLOB-ANT v4.2 inventory (https://eccad.aeris-data.fr/) provided by the Copernicus Atmosphere Monitoring Service (CAMS) to account for the anthropogenic emissions in the Asian areas outside China. To explore the sensitivity of secondary pollution and of *AOC* to emission reduction, several sensitivity experiments are designed based on our emissions inputs of NO_x, anthropogenic VOCs (AVOCs). As shown in Table S1 of the Supplementary Information, NO_x emissions include the emissions of NO_2 and NO, AVOCs emissions include those of alkanes [ethane (C_2H_6), propane (C_3H_8), and BIGALK (alkanes with carbon number $\geqslant 4$)], alkenes [ethene (C_2H_4), propene (C_3H_6), and BIGENE (alkenes with carbon number$\geqslant$4)], aromatics [benzene (C_6H_6), toluene ($C_6H_5CH_3$), and xylene ($C_6H_4(CH_3)_2$))], alkyne (C_2H_2), isoprene (C_5H_8), terpenes ($C_{10}H_{16}$), and OVOCs [methanol (CH_3OH), ethanol (C_2H_5OH), acetaldehyde (CH_3CHO), acetone (CH_3COCH_3), methacrolein (CH_2CCH_3CHO; MACR), and methyl vinyl ketone ($CH_2CHCOCH_3$; MVK)]. The emissions of ammonia (NH_3), sulfur dioxide (SO_2), and carbon monoxide (CO) are also considered.

2.2. Design of numerical experiment

To explore the sensitivity of secondary pollutants to emissions changes, five numerical experiments are conducted for January and July of 2018, respectively (Table 1). In the baseline case, denoted as "*BASE*", we adopt the emissions described in Sect. 2.1. The concentrations of the key species calculated in this specific case have been validated in our companion study (Dai et al., 2023). To quantify the sensitivity of pollutants to potential mitigation policies, we apply uniform reductions in the surface emissions of primary pollutants over the entire geographical area of China; In the first two cases, arbitrary 50% reductions are applied separately to the NO_x and AVOCs emissions relative to the baseline case. These two cases are labeled "*NO_x*" and "*AVOCs*", respectively. A third case in which the 50% reduction is applied to both NO_x and AVOCs emissions is referred to as "*N+A*". The difference between the "perturbed" concentrations of pollutants and chemical parameters relative to the baseline case provides an estimate of the response in secondary pollution and chemistry to emission reduction.

Additionally, a simulation labeled "*TOTAL*" assumes that all anthropogenic emissions under consideration (NO_x, AVOCs, CO, SO_2, and NH_3) are simultaneously reduced by 50%. This particular case is used to explore the impact on the ozone formation of a reduction in the emission of CO (an ozone precursor) and of SO_2 and NH_3 (as aerosol precursors). The spatial distribution of the changes in the emission fluxes for the different cases is shown in Fig. S1.

3. **Model results**

3.1 Response of ozone concentrations to emission reduction

First, we describe the changes in the surface concentration of ozone in response to the reduction applied to the surface emissions. To support the discussion, we adopt an indicator to distinguish different ozone sensitivity regimes. This indicator is defined as the calculated ratio between the production rate of hydrogen peroxide (H_2O_2) and of nitric acid (HNO_3) [$P(H_2O_2)/P(HNO_3)$]. An area is assumed to be VOC-limited or NO_x-limited if the adopted indicator $P(H_2O_2)/P(HNO_3)$ is smaller than 0.06 or if it is larger than 0.2, respectively (Tonnesen and Dennis, 2000; Yang et al., 2020; Zhao et al., 2019; Dai et al., 2023). The regions with ratios between these two limits represent transition situations.

Figure 1 displays the spatial distribution of the changes in the surface concentration of ozone during daytime (06:00 to 19:00 Local Standard Time) resulting from a 50% reduction in the emissions of NO_x, AVOCs, combined NO_x and AVOCs, and the additional reduction in other anthropogenic species (NH_3, SO_2, and CO) for January and July 2018.

Winter conditions. In January, the 50% reduction in the NO_x emissions (*NOx* case) enhances the surface ozone concentrations, with the largest increase derived in the YRD and PRD regions by 15%−33% (6−12 ppbv; Fig. 1a). During wintertime, a large part of China is under a VOC-sensitive regime (Fig. S2a). The reduced ozone titration due to NO_x emission reduction leads to a decrease in ozone destruction (Fig. S3a) and hence favors an increase in the ozone concentration. If AVOCs emissions are reduced by 50% (*AVOCs* case), the surface ozone concentration is reduced by 4%−10% (2.0 to 8.0 ppbv; Fig. 1b) in South China. This ozone decrease is associated with reduced levels of radicals (see Sec. 3.2.1) and hence a reduction in the ozone production (Fig. S4a).

In the case with a combined emission reduction (*N+A* case), the ozone response in VOC-limited areas follows the positive changes found in the NO_x-reduction case, with an ozone increase of 4%−9% (3.0−7.5 ppbv; Fig. 1c) in North China and in some urban regions in South China. Simultaneously, a slight decrease in the ozone concentration is derived along the coast of South China (5%−8% or 2.0−4.5 ppbv). In these areas, the ozone sensitivity is under the control of the NO_x. The ozone decrease is dominated by the negative ozone response to the AVOCs emission reduction. With a further emission reduction for the other chemical species (*TOTAL* case), an ozone increase (4%−6% or 3−5 ppbv; Fig. 1d) relative to the combined case is calculated in South China.

Summer conditions. In July, under the reduction in the NO_x emissions, an increase in the surface ozone concentration of up to 17% (10 ppbv; Fig. 1e) is calculated in the urbanized regions of North China Plain (NCP), YRD, and PRD. These areas are typically located in VOC-limited areas (Fig. S2b); thus, the ozone increase is explained by the reduced ozone titration due to NO_x emission reduction. At the same time, in NO_x-limited areas, the calculated surface ozone concentration is reduced by 3%−10% (2 to 8 ppbv), in response to the reduced photochemical formation under lower NO_x concentrations. With the reduction of AVOCs emissions, the surface concentration of ozone decreases by 8%−20% (8.0−12.0 ppbv; Fig. 1f) in all areas of China.

In the combined emission reduction case, the surface concentration of ozone decreases by up to 15% (12 ppbv; Fig. 1g) in the NO_x-sensitive areas. In the VOC-sensitive areas, the surface ozone concentration also decreases, which differs from the ozone changes derived for winter conditions. This is explained by the fact that the loss of ozone due to NO_x titration is rapidly compensated by the photochemical formation of ozone, as the ozone production rate is enhanced by high temperatures and by large photolysis rates during summertime (T. Wang et al., 2022). When the emission reduction is applied to all species under consideration, the ozone changes (Fig. 1h) relative to the combined case are smaller than the changes derived in winter, due to a consistently smaller reduction in aerosol concentrations (see Sec. 3.2.3).

Table 2 and Figure S5 provide quantitative information on the response of ozone to emission reduction at four urban locations (Beijing, Shanghai, Chengdu, and Guangzhou) for January and July of 2018. In winter (in January), the reduction in the emission of NO_x results in ozone

increases of 21.3%−33.2% in all cities, while the reduction applied to AVOCs emission results in a decrease of urban ozone levels by 2.5%−18.2%. Ozone changes in the *N+A* and *TOTAL* cases follow the ozone response found in the *NOx* case, with concentration increases of 7.1%−22.0% and of 10.0%−22.7%, respectively. In summer (in July), the urban ozone responses to the *NOx* and *AVOCs* cases are similar to those derived for winter conditions. The calculated ozone concentrations increase by 5.5%−17.1% in response to the reduced NO_x emissions and decrease by 14.5%−22.9% in response to the reduced AVOCs emissions. In the *N+A* and *TOTAL* cases, the changes in the ozone concentration follow the response to *AVOCs* reductions: the ozone concentration decreases at the sites of Beijing (by 5.5% and by 7.3%), Shanghai (by 2.9% and 2.6%), and Chengdu (by 3% and 2.5%). An exception is found at the Guangzhou site, where the ozone concentration increases by 1.3% in both cases; this calls for a different role of the anthropogenic emissions regarding the ozone formation at this location.

3.2. Changes in precursors and intermediates in ozone formation

In this section, we describe the changes in the surface concentration of ozone precursors and intermediates in response to the reduction in surface emissions. We focus in particular on the hydroxyl radical (OH), the hydroperoxyl radical (HO_2), specific oxidized volatile organic compounds (OVOCs) species, as well as secondary aerosols

3.2.1. Changes in radicals

To support the discussion on the radical changes induced by the emission reduction, we examine the changes in the values of two specific parameters: the production rate of peroxy radicals (RO_x=OH+HO_2+RO_2; $P(RO_x)$) and the destruction rate of these radicals ($D(RO_x)$) (Tan et al., 2019). The production rate of RO_x radicals ($P(RO_x)$) includes the photolysis of O_3, of nitrous acid (HONO), and of different OVOCs species, as well as the ozonolysis of alkenes. The destruction rate of RO_x radicals ($D(RO_x)$) results from the termination reactions between different RO_x radicals, and between RO_x radicals and nitric oxide. Another loss process for hydroperoxy radicals is provided by the heterogeneous uptake of HO_2 on aerosol surfaces. Detailed model estimates of $P(RO_x)$ and $D(RO_x)$ can be found in Part 1 of the present study (Dai et al., 2023).

Winter conditions. Figure 2 displays the spatial distribution of the changes in the surface daytime (06:00 to 19:00 LST) mixing ratios of OH and HO_2 radicals resulting from a 50% reduction in the emissions of NO_x, AVOCs, combined NO_x and AVOCs, and additional species (NH_3, SO_2, and CO) for January 2018. With the reduction in NO_x emissions (*NOx* case), the calculated mixing ratio of the surface OH radical is reduced in South China by up to 40% (0.05 pptv; Fig. 2a), with a lower decrease in the central and western parts of the country. The reduction in the levels of the OH radical are due to the reduced oxidative capacity of the atmosphere associated with the NO_x emission reduction. The reduction in the atmospheric oxidative capacity is attributable to the decreases in the concentration of NO_2 (Fig. S6a) and of ozone.

At the same time, an increase in the mixing ratios of OH radicals is found in urban areas, including the NCP, YRD, PRD, and Si Chuan Basin (SCB) regions, with a maximum increase of 24% in the PRD region. Consistently, at the four city sites under consideration, the highest increase in the level of the OH radical is found at the Guangzhou site (Figure S7). This increase results from the reduced loss of the OH radical by the reaction with NO_2 (Fig. S6b).

A distinct increase in the surface mixing ratio of the HO_2 radical is derived in South China; it reaches 5 pptv or 60% (Fig. 2e). This increase contributes to a higher ozone level through the reaction between HO_2 and NO. The enhancement in the urban HO_2 concentration results from the increased levels of the OH radical via VOCs oxidation. The reduction in the aerosol load derived in South China as a result of the reduced NO_x emission is responsible for the reduced loss of HO_2 by aerosol uptake (see Sect. 3.2.3).

For the 50% decrease in AVOCs emissions (*AVOCs* case), the mixing ratios of OH and HO_2 radicals are reduced in South China by 4%−12% (0.005−0.015 pptv; Fig. 2b) and by 20%−36% (1−3 pptv; Fig. 2f), respectively. The decrease in the levels of these radicals is related to the reduced oxidation rate of VOCs following the decrease in the emissions and hence in the concentrations of hydrocarbons (Fig. S8a). The production of RO_x also decreases, especially from the reduced photolysis of formaldehyde (HCHO) and of other OVOCs (Fig. S8b, c), a consequence of the reduced AVOCs emissions. In the *AVOCs* case, the decreases in the radical levels and in the production rate of radicals explain the wintertime ozone decreases derived in South China. Simultaneously, a slight increase in the mixing ratio of the OH radical is derived.

This increase is related to the reduced extinction of solar radiation associated with the reduced aerosol load following the reduction in the AVOCs emissions.

When the 50% emission reduction in NO_x is combined with the 50% reduction in AVOCs emissions (*N+A* case), the distribution of changes in the OH radical is similar to the pattern induced by emission reduction in NO_x alone. However, a weakened increase is calculated, as the increase in the OH radical concentration with the reduced NO_x emissions is largely compensated by the decrease in the radical concentrations produced by the reduction in the AVOCs emissions. As shown in Fig. 2c, the maximum increase of the OH radical in urban China is reduced to 12% (from 40%). At the same time, the increases in the mixing ratio of the HO_2 radicals is reduced to 20% (from 60%; Fig. 2g), with only a mild increase distributed along the coast of South China. This compensating effect of the combined emission reduction on the radical levels is also reflected in the changes of the ozone concentrations, highlighting a link between the variations in the concentration of photochemical radicals and in the formation rate of ozone.

When accounting for the additional reduction in the emissions of other anthropogenic species (NH_3, SO_2, and CO) (*TOTAL* case), the mixing ratio of the OH radical is positively modified, relative to the results obtained in the combined case (*N+A* case). As shown in Fig. 2d, the mixing ratio of the OH radical is enhanced by up to 22% in the PRD and SCB regions. This increase is due to the reduced consumption of the OH radical by the reduced emissions and related concentrations of carbon monoxide (CO) (Fig. S9a and S1d). For the HO_2 radicals, the additional reduction in the other emissions contributes to a larger mixing ratio, with a pronounced increase in South China (by up to 18%; Fig. 2h). This increase in the HO_2 radical mixing ratio is due to the increased oxidation of the VOCs by the OH radical and the reduced aerosol uptake of HO_2 associated with the decrease in the aerosol load. The consistent increase between the OH and HO_2 radical levels and the ozone concentrations in South China reveals a positive relation between radical enhancement and ozone production.

Summer conditions. Figure 3 displays the spatial distribution of the changes in the daytime surface mixing ratio of the OH and HO_2 radicals due to the applied reduction in the emissions of NO_x, AVOCs, combined NO_x and AVOCs, and additional species for July 2018. When applying a 50% reduction in the NO_x emissions, the mixing ratio of the OH radicals decrease in large parts of China, with the maximum decrease reaching 40% (0.15 pptv; Fig. 3a). The

decrease in the concentration of the OH radicals can also be explained by the reduced consumption of OH by the reaction with NO_2, due to the reduced emissions of nitrogen oxides. The geographical area in which the concentration of OH radicals is reduced, covers a large fraction of China, including the northern provinces. This area is different from the wintertime situation, when the OH reduction was occurring only in South China. The concentration of the OH radical increases in the metropolitan areas, including in the YRD and PRD regions. A consistent increase in the concentrations of the OH radicals is also derived at the sites of Shanghai and Guangzhou (Fig. S7). Simultaneously, the surface mixing ratio of the HO_2 radical increases by 15%−20% (6−8 pptv; Fig. 3e) in the North China Plain, due to the reduced loss via aerosol uptake. The spatial shift in the distribution of radical changes from South China in winter to North China in summer is influenced by seasonal patterns of meteorological parameters, including temperature, water vapor abundance, and solar radiation intensity, which affect the atmospheric oxidative processes (Dai et al., 2023).

When AVOCs emissions are reduced by 50%, the mixing ratio of the radicals in urban areas, including in the NCP, YRD, and PRD regions, decreases on average by 8−12% in the case of OH (0.03−0.05 pptv; Fig. 3b) and by 6%−10% in the case of HO_2 (3−5 pptv; Fig. 3f). When applying the combined 50% emission reduction in AVOCs and NO_x, the changes in the patterns of the OH radical are similar to the distribution derived for the reduction in NO_x emissions alone, but it is also partially offset by the counteracting effect of AVOCs emissions, as for winter conditions. As shown in Fig. 3c, the maximum increase in OH radical is reduced to 20% (from 40%) and the maximum decrease is reduced to 12% (from 30%). The counteracting effect of AVOCs emission reduction is also shown in the enhanced abundance of HO_2 radicals (Fig. 3g), with less than 6% (from 15%−20%) increases in the urban areas.

With an additional 50% reduction in other anthropogenic emissions, the changes in OH and HO_2 radicals relative to the results obtained in the combined case are smaller than the changes derived for winter conditions (Fig. 3d and h). This is due to the small decrease in aerosol load during summer (see Sec. 3.2.3).

3.2.2 Changes in OVOCs

Oxygenated hydrocarbons (OVOCs) originate from direct biogenic and anthropogenic surface emissions (primary source), and from the oxidation of primary hydrocarbons (secondary

source) in the atmosphere (W. Wang et al., 2022). The photolysis of OVOCs produces photochemical radicals, which enter into the formation of secondary pollutants and have a potential negative effect on ozone pollution mitigation.

Winter conditions. Figure 4 shows the spatial distribution of the calculated changes in total OVOCs due to a 50% reduction in the emission of NO_x, AVOCs, combined NO_x and AVOCs, and additional other species for January 2018. With the adopted reduction in NO_x emission, the OVOCs concentration decreases in the non-urban areas of South China and increases in urbanized China (Fig. 4a), which is consistent with the changes derived for the mixing ratio of the OH radical. The highest increase in the OVOCs concentration is approximately 10% (2 ppbv) in the urban areas of the YRD and PRD regions; it includes a significant increase in the concentration of formaldehyde (HCHO; Fig. S10a), followed by peroxyacetyl nitrate (PAN; Fig. S10b), and alcohols (CH_3OH and C_2H_5OH; Fig. S10c), as the secondary formation of these OVOCs species is determined by the OH-related reactions (Emmons et al., 2010). At the four city sites under consideration, the highest increase in OVOCs is calculated at Shanghai and Guangzhou, with concentrations increasing by about 12% (1.8 ppbv; Fig. 4f) and 8% (1.2 ppbv; Fig. 4g), respectively. This increase in the concentration of OVOCs is consistent with the higher increase of OH radicals at these two sites (Fig. S7).

When the AVOCs emissions are reduced, the abundance of OVOCs is reduced in all regions of China (Fig. 4b), with the highest decrease found in the regions of PRD and SCB. At the four city sites under consideration (Fig. 4e-h), the decrease is most pronounced in the case of the concentration of ketones (see Table S2 for specific OVOCs speciation), including acetone (CH_3COCH_3), methyl vinyl ketone ($CH_3C(O)CHCH_2$), and methyl ethyl ketone ($CH_3CH_3C(O)CH_2CH_3$). The abundance of these species is reduced by nearly half, as the relevant ketones originate primarily from anthropogenic emissions. When combining the emission reduction of AVOCs and NO_x, the decrease in OVOCs concentration resulting from the AVOCs emission reduction is further strengthened in large areas of China (Fig. 4c). With additional decreases in the other emissions, the OVOCs' concentration is enhanced by 2−4 ppbv in whole China (Fig. 4d), which is consistent with the increased abundance of the OH radical resulting from a reduction in the NH_3, SO_2, and CO emissions.

Summer conditions. Figure 5 displays the spatial distribution of the changes in total OVOCs concentrations in response to a 50% reduction in the emission of NO_x, AVOCs, combined NO_x

and AVOCs, and additional species for July 2018. With a 50% reduction in NO_x emissions, a slight decrease in the OVOC's concentrations (0.5−1.5 ppbv or 3%−8%) is derived in South China (Fig. 5a), which is dominantly contributed by the decreases in the concentration of HCHO, glyoxal, and PAN (Fig. S11a-c). The decreases in these OVOCs species are due to a lower contribution from the secondary formation from OH-related reactions, as a consistent decrease is calculated for the changes in OH radical. However, in Central and North China, the calculated concentration of OVOCs generally increases (0.5−2.0 ppbv or 5%−8%). This increase is mainly contributed by the enhancement in the concentration of aldehydes (Fig. S12a) and alcohols (Fig. S12b). The increase of OVOCs species is possibly due to the enhanced contribution from the reactions between alkenes and isoprene, whose concentrations are increased (Fig. S12c, d), and enhanced oxidants. This result indicates that reducing anthropogenic emissions of aldehydes and alcohols may help offset the increase in OVOCs caused by the reduction in NO_x emissions.

With a 50% reduction in AVOCs emission, the OVOCs concentrations are significantly reduced in the NCP and SCB regions (by 20%−30% on average; Fig. 5b). Compared with the reduced OVOCs concentration (by 50%) in winter, the summertime response of OVOCs to the AVOCs emission reduction is smaller. Consistently, at the Beijing site (Fig. 5e), the decrease in OVOCs concentration is calculated by 30% (10 ppbv) on average, which is smaller than the decrease of 46% (5 ppbv) in winter. This seasonal difference is attributable to the higher photochemical formation of OVOCs during summertime, which is favored by the higher levels of temperature, solar radiation, as well as the temperature-dependent biogenic emissions. The smaller decrease in alcohols concentration (from 1.5 ppbv in winter to 0.5 ppbv in summer; Figure S13) is also supportive to our founding, as its summertime formation is highly dependent on the photochemically reactions with BVOCs (Zhang et al., 2023). Considering the increases in aldehydes and alcohols levels induced by reduced NO_x emission, this result also reveals a need to reduce the primary emissions of these two OVOCs to effectively control their negative impact on ozone pollution mitigation.

When the combined reduction in the emissions of AVOCs with NO_x is considered, a lower decrease (by 15%−26%; Fig. 5c) is found in the concentration of OVOCs in the geographical areas of China compared to the response derived for the individual reductions in the NO_x or AVOCs emissions. This response is consistent with the relevant changes in levels of OH radicals. When the emission reduction is applied to the other species under consideration, the

response of the OVOCs concentration to the reduced emissions is small (<2 ppbv or 5%; Fig. 5d).

3.2.3. Changes in aerosol

Figure 6 shows the changes in the average concentrations of secondary aerosol resulting from a 50% reduction in the emission of NO_x, AVOCs, combined NO_x and AVOCs, and additional other species in January and July of 2018.

Winter conditions. In January, the 50% reduction applied to NO_x leads to a large decrease in the aerosol load (10−18 μg m^{-3} or 12%−20%; Fig. 6a) in Central and South China. The aerosol decrease predominantly results from the decrease in the NO_3^- abundance (Fig. S14a) linked to the reduced concentration of NO_2, followed by the reduction in the concentration of NH_4^+ (Fig. S14b). A slight increase in the abundance of secondary organic aerosols (SOA) is derived in the urban areas of the NCP, YRD, and PRD regions (1−2 μg m^{-3} or 3%−5%; Fig. S14c), which is consistent with the increase in the level of oxidants, including the ozone and OH radicals. With a 50% reduction applied to AVOCs emissions, the changes in the aerosol concentration are smaller than with the 50% reduction applied to the NO_x emissions. The corresponding aerosol decrease of less than 4% (5 μg m^{-3}; Fig. 6b), predominantly results from the reduction in SOA concentrations (Fig. S15a). With a joint reduction in the emissions of NO_x and AVOCs (Fig. 6c), the decrease in the aerosol burden is larger than from the separated decrease in the individual emissions; this is explained by the fact that the increase in the concentration of SOA resulting from the reduced NO_x emissions is compensated by the reduced AVOCs emissions.

With a further reduction applied to other emissions (*TOTAL* case), the decrease in the concentration of aerosol is deeply enhanced in South China (Fig. 6d). This results in large part from the decrease in NO_3^- particles (by 5 μg m^{-3}; by Fig. S16c), followed by the decrease in the concentration of NH_4^+ (by 2 μg m^{-3}; Fig. S16a), SO_4^{2-} (by 1 μg m^{-3}; Fig. S16b). The decreases in NH_4^+ and SO_4^{2-} concentrations are due to the reduction in the concentration of their gas-phase precursors, NH_3 and SO_2. The decrease in the abundance of NO_3^- results from the formation of ammonium nitrate (NH_4NO_3) through the reaction of NH_3 with HNO_3 (Meng et al., 2022). This decrease in the aerosol burden explains the enhancement of HO_2 radicals since the aerosol uptake is reduced. This, in turn, promotes an increase in the ozone concentration in South China. At four city sites, the largest decrease in the aerosol

concentration is found at the Beijing site (Fig. S17), followed by the Chengdu site. This is attributed to the relatively high aerosol levels at these two locations. In our model, the concentrations of NO_2 and $PM_{2.5}$ are overestimated for the baseline conditions (Dai et al., 2023), which can possibly lead to an excessively high reduction in aerosol concentration, especially in the concentration of NO_3^-. This overestimation potentially affects the aerosol-related changes in the ozone formation.

Summer conditions. In July, the decrease in the aerosol load due to the emission reduction is much smaller than in winter. The reduction ranges from 1.5 to 5 μg m^{-3} (Fig. 6e), from 2 to 6 μg m^{-3} (Fig. 6f), from 4 to 7 μg m^{-3} (Fig. 6g) and from 8 to 10 μg m^{-3} (Fig. 6h), for the reduction in the *NOx*, *AVOCs*, *N+A*, and *TOTAL* emissions conditions, respectively. As for ozone, the reduction in aerosols also undergoes a spatial shift, from South China in winter to North China in summer. This shift is consistent with the calculated changes in oxidants, hydrocarbons, and other gaseous aerosol precursors. The higher decrease in the aerosol load for the combined case also indicates that the reduction in AVOCs emission increases the efficiency of the aerosol decrease produced by the reduced NO_x emissions.

The aerosol effect on ozone formation has been discussed in several modeling studies (Li et al., 2019; Liu et al., 2020; Dai et al., 2023). Our results show that the reduction in primary emissions results in a large decrease in aerosol concentrations. The major contribution to the aerosol decreases results from the reduction in NO_x emissions, with a strengthened effect when combined with a reduction in the AVOCs emissions. This decrease in the aerosol burden weakens the aerosol extinction effect and therefore enhances the photochemical formation rate of radicals and ozone. As shown in Fig. S18a-d, the photolysis rate increases (by 5%-20%) in Central and South China during winter due to the aerosol decrease induced by the emission reductions. The highest increase in the photolysis rates results from the joint emission reduction in NO_x and AVOCs (Fig. S18c). The increase of the photolysis rates in summer is not as distinct as the increase during wintertime due to the limited reduction in the aerosol burden during summer (Fig. S18e-h).

Further, the reduction in the aerosol burden lowers the aerosol uptake of NO_2 and HO_2 radicals, which indirectly enhances the mixing ratio of OH and HO_2 radicals (Dai et al., 2023). An increased level of HO_2 radical following the emission reduction is caused by the reduced aerosol uptake. Large uncertainties still exist in the adopted value of the uptake coefficient of

HO_2 (considered as 0.1 in this study) (Yang et al., 2023). This affects the quantitative evaluation of the aerosol effects on the ozone levels and deserves further studies. Considering the impact of aerosol load on ozone formation, it is essential to account for the aerosol effect on ozone formation, even with stringent emission reductions in the future.

3.3. Response of ozone sensitivity regimes to emission reduction

Figure 7 displays the spatial distribution of ozone regimes in response to applied emission reductions for of NO_x, AVOCs, for combined NO_x and AVOCs (*N+A*), and for additional species (*TOTAL*) in January and July.

Winter conditions. In January, when a 50% reduction is applied to the NO_x emissions, the regions characterizing the ozone production in the south and southwest of China (in *BASE* case; Fig. S2a) tend to be converted from transition or VOC-limited regimes to NO_x-limited areas (from 68.8% in *BASE* case to 71.9% in *NOx* case; Table S3) (Fig. 7a). The change in the ozone sensitivity regimes is consistent with (1) the reduced HNO_3 concentration (Fig. S19a) due to less NO_2 reacting with OH, and (2) the enhanced H_2O_2 concentration (Fig. S10e) due to the reduced aerosol HO_2 uptake by aerosol particles. With a 50% reduction applied to the AVOCs emissions, some transition areas of South China are converted to VOC-limited areas (Fig. 7b; from 20.1% in the *BASE* case to 21.3% in the *AVOCs* case). A relevant decrease in the H_2O_2 concentration, derived in South China (Fig. S19f), is attributed to the decrease in the calculated HO_2 concentration. When considering the combined reduction in NO_x and AVOCs emissions as well as the reduction in all anthropogenic emissions, the VOC-limited regions of South China evolve towards a transition region or even a NO_x-limited region (Fig. 7c; Fig. 7d). In these two last cases, the changes in ozone sensitivity regimes are determined by the decrease in the calculated HNO_3 concentrations (Fig. S19c, d). At the urban sites, the emission reduction does not modify the wintertime ozone sensitivity regimes (Fig. S20), which remain VOC-limited.

Summer conditions. In July, the changes in ozone regimes related to emission reductions are found mainly in VOC-limited areas and their surroundings, due to consistent changes in H_2O_2 and HNO_3 (Fig. S21). With the reduction of NO_x emissions, the size of VOC-limited areas shrinks and becomes a smaller fraction of the urbanized areas (Fig. 7e; from 3.4% in the *BASE* case to 2.9% in the *NOx* case). The regimes at three urban sites, which are VOC-limited in the

BASE case, are modified: the ozone sensitivity at Beijing is converted to a NO_x-limited case (Fig. 7i), while the sites of Shanghai (Fig. 7j) and Chengdu (Fig. 7l) are shifted towards a Transition regime. The changes in ozone sensitivity at these three city sites result from the decreased production of HNO_3 due to reduced NO_2 as well as the increased production of H_2O_2 due to reduced HO_2 loss via aerosol uptake. The Guangzhou site remains in a VOC-limited region (Fig. 7k). Reasons for this exception can be the lower aerosol load (Fig. S17) and higher temperature-dependent biogenic VOCs emissions in the location (Dai et al., 2023), as its surroundings are covered by vegetations (Zhang et al., 2023).

With the reduction in AVOCs emissions, the VOC-limited areas expand to the surroundings of the metropolitan areas (Fig. 7g; 3.7% in *AVOCs* case). Finally, when applying a combined 50% reduction in the emissions of NO_x and AVOCs (*N+A* case; Fig. 7g) as well as the reduction of all other emitted species (*TOTAL* case; Fig. 7h), the patterns of the calculated change in the ozone sensitivity are similar to the pattern corresponding to the NO_x emissions; specifically, the VOC-limited area (3.0% in *N+A* and *TOTAL* case) becomes smaller relative to the *BASE* case. In these cases, the sites of Beijing and Chengdu shift to a transition condition, while the Guangzhou and Shanghai sites remain under VOC-limited conditions. This result is consistent with the ozone increase obtained for the *N+A* and *TOTAL* cases at the Guangzhou sites.

3.4. Changes in Atmospheric Oxidative Capacity

The atmospheric oxidizing capacity (*AOC*) characterizes the self-cleansing ability of the atmosphere (Dai et al., 2023). This parameter is expressed as:

$$AOC = \sum_i^j k_{i,j}[Y_i][X_j].$$

Here the $k_{i,j}$ represents the reaction rate between carbon monoxide (CO), methane (CH_4), and non-methane hydrocarbons (NMHCs) (noted here as Y_i) and the OH radical, the NO_3 radical as well as O_3 (noted as X_j).

The changes in the spatial distribution of daytime (06:00 to 19:00 LST) *AOC* resulting from the adopted 50% reduction in the emissions of ozone precursors for January and July of 2018 are depicted in Fig. 8.

Winter conditions. In January, the 50% reduction in NO_x emission leads to a decrease in daytime *AOC* of 10%−20% in South China and an increase of 10%−18% in the urban areas, including the PRD, YRD and, SCB regions (Fig. 8a). At the four city sites (Fig. 9a-d), the increase in the daytime *AOC* is attributed to the enhanced contributions of the OH-related reactions, including the reactions of OH with alkenes, followed by the reaction of OH with OVOCs and with aromatics. This daytime increase in *AOC* is consistent with the enhanced level in the OH radical, alkenes, and OVOCs when the NO_x emissions are reduced. The change in *AOC* with NO_x emission reduction allows us to characterize the formation process of O_3 and can be used as an indicator to design mitigation policies for reducing ozone pollution. During nighttime (20:00 to 05:00 LST), the reduction in NO_x emissions is responsible for an increase in *AOC* by up to 50% (Fig. S22a). A contribution to this increase is provided by the alkenes' ozonolysis, since the concentration of ozone (Fig. 6a) and of alkenes is enhanced (Fig. S12c). The largest increase in the alkene ozonolysis (from 31% to 40%, see Fig. S23b) is derived at the site of Shanghai. These results highlight the enhanced oxidative processes associated with the NO_x emission reduction.

With the 50% reduction in AVOCs emissions, the daytime *AOC* is reduced in all the major regions of China (Fig. 8b), with the largest decreases occurring in the southern part of the country; specifically, the largest decrease occurs at the Guangzhou site (by 50%). This decrease in daytime *AOC* is mainly attributable to the reduced contribution from the reactions between OH and alkenes, followed by the reactions of OH with aromatics and with OVOCs. With a combined reduction in the emissions of NO_x and AVOCs (*N+A*; Fig. 8c), the distribution patterns of the changes in daytime *AOC* are similar to the patterns found in the *AVOCs* cases but are characterized by higher decreases in daytime *AOC*. With the additional reduction in the other emissions considered here (*TOTAL*; Fig. 8d), an increase (relative to the *BASE* case) of daytime *AOC* is derived in central and south China; this result is consistent with the increase of OH radical levels and of the ozone concentrations.

Summer conditions. During summertime, the decrease in daytime *AOC* is more pronounced than during wintertime. With the 50% reduction applied to NO_x emissions, the daytime *AOC* decreases in large areas of China (ranging from 10%−20%; Fig. 8e), while, in urban areas, an increase is predicted, including at the Guangzhou (8%; Fig. 9g), Shanghai (5%; Fig. 9f), and Chengdu (3%; Fig. 9h) sites. However, at the Beijing site, the daytime value of *AOC* decreases

(Fig. 9e), because of the shift in the ozone sensitivity regime (from VOC-limited to NO_x-limited conditions). During nighttime, the NO_x emission reduction also leads to an increase in *AOC* due to the alkene ozonolysis (Fig. S22b), with the largest increase derived at the Beijing site (from 10% to 14%; Fig. S23e).

With other emission reduction cases (*AVOCs* and *N+A*; Fig. 8f, g), the daytime *AOC* decreases in entire China, with more distinct decreases (relative to winter conditions) occurring in North China. With the reduction in the AVOCs emissions, the relative decrease of daytime *AOC* is smaller than in winter, especially at the Guangzhou site (to 30%), indicating a more important secondary formation of VOC-related *AOC* during summer. When the emissions of NO_x and AVOCs are jointly reduced by 50%, the role of the reaction between OH and BVOCs in the determination of *AOC* is enhanced at the four city sites, with the largest increase (15%) found at the Guangzhou site. This increase results from the enhanced levels of OH radicals (Fig. 2c) and in the presence of biogenic VOCs species, such as isoprene (Fig. S24).

The distribution patterns of changes in daytime *AOC* due to emission reduction are largely consistent with the changes in the mixing ratio of the OH radicals and the changes in the concentration of OVOCs, ozone, and SOA in both winter and summer. These consistent patterns suggest that the *AOC* is an appropriate indicator to characterize the changes in secondary pollutants attributed to emission reduction. One exception is found when considering the changes in the ozone concentration resulting from the reduction in NO_x emissions during winter. During this season, a comparison between the values of daytime *AOC* and the changes in the ozone concentration (Fig. 5a) suggests that the change in daytime *AOC* reflects primarily the changes in the net production rate of odd oxygen (Fig. S25); this can be explained by the important role played by NO_2 in the wintertime formation of ozone.

4. Summary and Policy Implications

The model simulations performed in the present study explore the response of radicals, ozone, and the atmospheric oxidative processes to a 50% reduction applied to the primary emissions of key pollutants. Our analysis provides insight into the changes affecting ozone chemistry and the oxidizing processes to be expected in response to future emission reduction.

In winter, as most geographical areas are VOC-limited (saturated in NO_x) a 50% reduction in NO_x emissions leads to an ozone concentration increase of up to 8−10 ppbv (15%−25%) in all geographical regions of China; this increase results from of the reduced titration of ozone by nitric oxide. When combining this NO_x reduction with a 50% reduction applied to AVOCs emissions, the ozone enhancement found in the rural areas and resulting from the reduced NO_x is considerably reduced. However, in urban areas (VOC-limited situation), the ozone increase, although weakened, still exists (by 3.0−7.5 ppbv).

In summer, as most rural areas of China become NO_x-limited, the geographical regions covered by the ozone increase in response to the 50% reduction applied to the NO_x emissions shrink almost to the VOC-limited metropolitan areas. In these urban environments, the ozone increase reaches a maximum of 10 ppbv or 17%. When the NO_x emission reduction is combined with a 50% reduction in the VOC emissions, the increase in ozone almost disappears in all areas of China. This is explained by the significant decrease in the ozone production resulting from the reduced levels of hydrocarbons. However, in the areas where hydrocarbons are primarily of biological origin, the ozone concentration (i.e., linked to the photochemical degradation of isoprene) still slightly increases (i.e., by 0.5 ppbv or 1.3% at the Guangzhou sites).

Paths to mitigation. We conclude this paper by highlighting a few chemical paths that should be considered when designing mitigation policies for the reduction of ozone in the urban areas of China. Figure 10 presents a schematic description of the chemical mechanisms involved in the chemical production of atmospheric ozone, and highlights how different reaction paths tend to change the ozone abundance in response to a reduction in NO_x and anthropogenic VOC (AVOCs) emissions. This graph shows that a reduction in NO_x emissions tends to increase the ozone concentration by (1) reducing the rate of the $NO + O_3$ reaction (ozone titration); (2) by increasing the rate of the $HO_2 + NO$ reaction due to an increase in the HO_2 level associated with the reduced uptake of this radical by a lowered aerosol load; (3) by increasing the atmospheric oxidizing capacity (*AOC*) through OH-related reactions. The graph also shows that a decrease in AVOCs emissions tends (1) to reduce the level of the HO_x radical and hence the ozone production by the $HO_2 + NO$ reaction; (2) to enhance the level of OH radical due to the reduced aerosol uptake and (3) to reduce the *AOC* with a negative change of the ozone concentration. The relative importance of these different chemical mechanisms varies with location and environmental conditions.

We conclude that in *winter*, when the background ozone concentration is low, the reduction of NO_x emissions tends to increase the level of near-surface ozone, while the reduction in AVOCs emissions has the opposite effect. This conclusion applies both in rural and in urban areas. A combined reduction in the emissions of these two primary pollutants tends to decrease the level of ozone in rural areas but to increase ozone in urban areas. Thus, in urban areas during winter, an effective approach to reduce the surface ozone concentration is through a strong limitation in the emissions of volatile organic compounds.

In *summer* when the ozone level is generally high, the reduction of NO_x emissions is an effective action to reduce the ozone concentration in rural areas. This measure, however, is counterproductive in the NO_x-saturated urban areas where ozone is controlled by VOCs. In fact, in urban areas during this season, the mechanisms involved in ozone mitigation are complex. For example, when NO_x emissions are reduced, the atmospheric OH concentration is enhanced because of its reduced destruction by NO_2. Following this increase in the OH concentration, an increase in the level of OVOCs, whose photolysis is an important source of HO_x radicals, also leads to accelerated ozone production and further amplifies the oxidation of VOCs. In addition, the increase in *AOC*, linked to the reactions of OH and ozone with alkenes and the reactions of OH with OVOCs also contribute to an increase in the ozone production. Further, the reduction in the aerosol load, resulting from a reduction in the emissions of aerosol precursors, promotes ozone formation by decreasing the aerosol extinction of light and by reducing the uptake of HO_2. If combined with a 50% reduction in AVOCs, the increase in the OVOCs concentrations and *AOC*, resulting from reduced NO_x emissions, can be offset. However, the aerosol-related promotion of the level of OH and HO_2 radicals can be enhanced, highlighting the complexity of summertime ozone mitigation in urban areas.

Overall, in urban areas, the reduction in the surface ozone levels requires a reduction in the emissions of anthropogenic VOCs. These results are consistent with the studies of W. Wang et al (2023) and Liu et al., (2023), who stated that the priority to control ozone pollution in China should be to reduce the emissions of VOCs. Our study assumes a uniform 50% reduction in the emissions of all primary VOCs. Future work should therefore determine which of these VOCs should be reduced as a priority to determine the most effective ozone control strategy. Our results suggest that reducing emissions of alkenes, aromatics, and unsaturated VOCs, especially methanol and ethanol, should be a priority. To develop efficient mitigation strategies

that reduce anthropogenic VOC emissions, more detailed investigations are needed into the reactivity of individual VOCs and their potential impact on urban ozone formation.

Code and data availability. The WRF-Chem model is publicly available at https://www2.mmm.ucar.edu/wrf/users/. The modified code in the WRF-Chem model is available upon request to the corresponding author. The air quality data at surface stations are publicly available at the website of the Ministry of Ecology and Environment of the People's Republic of China at http://english.mee.gov.cn/.

Author contributions. JD and GB designed the structure of the manuscript, performed the numerical experiments, analyzed the results, and wrote the manuscript. JD analyzed the data and established the figures. All co-authors provided comments and reviewed the manuscript.

Competing interests. The authors declare that they have no conflict of interest.

Acknowledgments. The present joint Sino-German study was supported by the German Research Foundation (Deutsche Forschungs Gemeinschaft DFG), the National Science Foundation of China (NSFC) under Air-Changes grant no. 4487-20203, the Research Grants Council– University Grants Committee (grant no. T24-504/17-N) and the NSFC (grant no.42293322). The National Center for Atmospheric Research (NCAR) is sponsored by the US National Science Foundation. We would like to acknowledge the high-performance computing support from NCAR Cheyenne.

References

China Air 2023, Air Pollution Prevention and Control Progress in Chinese Cities. http://www.allaboutair.cn/uploads/231027/ChinaAir2023EN.pdf

Dai, J., Brasseur, G. P., Vrekoussis, M., Kanakidou, M., Qu, K., Zhang, Y., Zhang, H., and Wang, T.: The atmospheric oxidizing capacity in China – Part 1: Roles of different photochemical processes, Atmos. Chem. Phys., 23, 14127–14158, https://doi.org/10.5194/acp-23-14127-2023, 2023.

Emmons, L. K., Walters, S., Hess, P. G., Lamarque, J.-F., Pfister, G. G., Fillmore, D., Granier, C., Guenther, A., Kinnison, D., Laepple, T., Orlando, J., Tie, X., Tyndall, G., Wiedinmyer, C., Baughcum, S. L., and Kloster, S.: Description and evaluation of the Model for Ozone and Related chemical Tracers, version 4 (MOZART-4), Geosci. Model Dev., 3, 43–67, https://doi.org/10.5194/gmd-3-43-2010, 2010.

Jacob, D. J., Horowitz, L. W., Munger, J. W., Heikes, B. G., Dickerson, R. R., Artz, R. S., and Keene, W. C.: Seasonal transition from NOx - to hydrocarbon-limited conditions for ozone production over the eastern United States in September, J. Geophys. Res.-Atmo., 100, 9315–9324, https://doi.org/10.1029/94JD03125, 1995.

Knote, C., Hodzic, A., Jimenez, J. L., Volkamer, R., Orlando, J. J., Baidar, S., Brioude, J., Fast, J., Gentner, D. R., Goldstein, A. H., Hayes, P. L., Knighton, W. B., Oetjen, H., Setyan, A., Stark, H., Thalman, R., Tyndall, G., Washenfelder, R., Waxman, E., and Zhang, Q.: Simulation of semi-explicit mechanisms of SOA formation from glyoxal in aerosol in a 3-D model, Atmos. Chem. Phys., 14, 6213–6239, https://doi.org/10.5194/acp-14-6213-2014, 2014.

Li, B., Ho, S.S.H., Li, X., Guo, L., Chen, A., Hu, L., Yang, Y., Chen, D., Lin, A., Fang, X., A comprehensive review on anthropogenic volatile organic compounds (VOCs) emission estimates in China: comparison and outlook. Environ. Int. 156, 106710, https://doi.org/10.1016/j.envint.2021.106710, 2021.

Li, C., Liu, Y., Cheng, B., Zhang, Y., Liu, X., Qu, Y., Feng, M.: A comprehensive investigation on volatile organic compounds (VOCs) in 2018 in Beijing, China: Characteristics, sources and behaviors in response to O3 formation. Sci. Total Environ, 806, 150247https://doi.org/10.1016/j.scitotenv.2021.150247, 2022.

Li, J., Xie, X., Li, L., Wang, X., Wang, H., Jing, S. A., Hu, J.: Fate of Oxygenated Volatile Organic Compounds in the Yangtze River Delta Region: Source Contributions and Impacts on the Atmospheric Oxidation Capacity. Environ. Sci., Technol., 56(16), 11212-11224.https://doi.org/10.1021/acs.est.2c00038, 2022.

Li, K., Jacob, D. J., Liao, H., Shen, L., Zhang, Q., Bates, K. H.: Anthropogenic drivers of 2013−2017 trends in summer surface ozone in China. Proc. Natl. Acad. Sci., 116 (2), 422−427, https://doi.org/10.1073/pnas.1812168116, 2019.

Li, K., Jacob, D. J., Liao, H., Qiu, Y., Shen, L., Zhai, S., Kuk, S. K.: Ozone pollution in the North China Plain spreading into the late-winter haze season. Proc. Natl. Acad. Sci., 118(10), e2015797118, https://doi.org/10.1073/pnas.2015797118, 2021.

Liu, T., Hong, Y., Li, M., Xu, L., Chen, J., Bian, Y., Yang, C., Dan, Y., Zhang, Y., Xue, L., Zhao, M., Huang, Z., and Wang, H.: Atmospheric oxidation capacity and ozone pollution mechanism in a coastal city of southeastern China: analysis of a typical photochemical episode by an observation-based model, Atmos. Chem. Phys., 22, 2173–2190, https://doi.org/10.5194/acp-22-2173-2022, 2022.

Liu, Y., Geng, G., Cheng, J., Liu, Y., Xiao, Q., Liu, L., Zhang, Q.: Drivers of Increasing Ozone during the Two Phases of Clean Air Actions in China 2013–2020. Environ. Sci., Technol., https://doi.org/10.1021/acs.est.3c00054, 2023

Liu, Y., and Wang Tao: Worsening urban ozone pollution in China from 2013 to 2017 – Part 2: The effects of emission changes and implications for multi-pollutant control, Atmos. Chem. Phys., 20, 6323-6337, https://doi.org/10.5194/acp-206323, 2020.

Meng, F., Zhang, Y., Kang, J., Heal, M. R., Reis, S., Wang, M., Liu, L., Wang, K., Yu, S., Li, P., Wei, J., Hou, Y., Zhang, Y., Liu, X., Cui, Z., Xu, W., and Zhang, F.: Trends in secondary inorganic aerosol pollution in China and its responses to emission controls of precursors in wintertime, Atmos. Chem. Phys., 22, 6291–6308, https://doi.org/10.5194/acp-22-6291-2022, 2022.

Ou, J., Yuan, Z., Zheng, J., Huang, Z., Shao, M., Li, Z., Louie, P. K.: Ambient ozone control in a photochemically active region: short-term despiking or long-term attainment? Environ. Sci., Technol., *50* (11), 5720-5728, https://doi.org/10.1021/acs.est.6b00345, 2016.

Skamarock, W.C., Klemp, J.B., Dudhia, J., Gill, D.O., Liu, Z., Berner, J., Wang, W., Powers, J.G., Duda, M.G., Barker, D.M.: A Description of the Advanced Research WRF Model Version 4; Mesoscale and Microscale Meteorology Laboratory NCAR: Boulder, CO, USA, 2019.

Song, H., Lu, K., Dong, H., Tan, Z., Chen, S., Zeng, L., Zhang, Y.: Reduced aerosol uptake of hydroperoxyl radical may increase the sensitivity of ozone production to volatile organic compounds. Environ. Sci., Technol. Lett., 9(1), 22-29. https://doi.org/10.1021/acs.estlett.1c00893, 2021.

Tan, Z., Lu, K., Hofzumahaus, A., Fuchs, H., Bohn, B., Holland, F., Liu, Y., Rohrer, F., Shao, M., Sun, K., Wu, Y., Zeng, L., Zhang, Y., Zou, Q., Kiendler-Scharr, A., Wahner, A., and Zhang, Y.: Experimental budgets of OH, HO_2, and RO_2 radicals and implications for ozone formation in the Pearl River Delta in China 2014, Atmos. Chem. Phys., 19, 7129–7150, https://doi.org/10.5194/acp-19-7129-2019, 2019.

Tan, Z., Lu, K., Ma, X., Chen, S., He, L., Huang, X., Zhang, Y.: Multiple Impacts of Aerosols on O3 Production Are Largely Compensated: A Case Study Shenzhen, China. Environ. Sci., Technol., 56(24), 17569-17580, https://doi.org/10.1021/acs.est.2c06217, 2022.

Tonnesen, G. S., and R. L. Dennis.: Analysis of radical propagation efficiency to assess ozone sensitivity to hydrocarbons and NO_x: 2. Long-lived species as indicators of ozone concentration sensitivity, *J. Geophys. Res.*, 105(D7), 9227–9241, https://doi.org/10.1029/1999JD900372, 2000.

Wang, J, Zhang Y, Xiao S, Wu Z, Wang X.: Ozone Formation at a Suburban Site in the Pearl River Delta Region, China: Role of Biogenic Volatile Organic Compounds. Atmosphere, 14 (4):609. https://doi.org/10.3390/atmos14040609, 2023.

Wang, T., Xue, L., Feng, Z., Dai, J., Zhang, Y., Tan, Y.: Ground-level ozone pollution in China: a synthesis of recent findings on influencing factors and impacts. Environ. Res. Letters, 17(6), 063003. https://doi.org/10.1088/1748-9326/ac69fe, 2022.

Wang, W., van der A, R., Ding, J., van Weele, M., and Cheng, T.: Spatial and temporal changes of the ozone sensitivity in China based on satellite and ground-based observations, Atmos. Chem. Phys., 21, 7253–7269, https://doi.org/10.5194/acp-21-7253-2021, 2021.

Wang, W., Yuan, B., Peng, Y., Su, H., Cheng, Y., Yang, S., Wu, C., Qi, J., Bao, F., Huangfu, Y., Wang, C., Ye, C., Wang, Z., Wang, B., Wang, X., Song, W., Hu, W., Cheng, P., Zhu, M., Zheng, J., and Shao, M.: Direct observations indicate photodegradable oxygenated volatile organic compounds (OVOCs) as larger contributors to radicals and ozone production in the atmosphere, Atmos. Chem. Phys., 22, 4117–4128, https://doi.org/10.5194/acp-22-4117-2022, 2022.

Wang, W., Li, X., Cheng, Y. Parrish, D. D., Ni, R., Tan, Z, Liu, Y., Lu, S., Wu, Y., Chen, S., Lu, K., Hu, M., Zeng, L., Shao, M., Huang, C., Tian, X., Leung, K., Chen, L., Fan, M., Zhang, Q., Rohrer, F., Wahner, A., Poschl, U., Su, H., Zhang, Y., Ozone pollution mitigation strategy informed by long-term trends of atmospheric oxidation capacity. *Nat. Geosci.* 17, 20–25 https://doi.org/10.1038/s41561-023-01334-9, 2024.

Xue, L., Gu, R., Wang, T., Wang, X., Saunders, S., Blake, D., Louie, P. K. K., Luk, C. W. Y., Simpson, I., Xu, Z., Wang, Z., Gao, Y., Lee, S., Mellouki, A., and Wang, W.: Oxidative capacity and radical chemistry in the polluted atmosphere of Hong Kong and Pearl River Delta region: analysis of a severe photochemical smog episode, Atmos. Chem. Phys., 16, 9891–9903, https://doi.org/10.5194/acp-16-9891-2016, 2016.

Yang, G., Liu, Y., Li, X. Spatiotemporal distribution of ground-level ozone in China at a city level. Sci Rep 10, 7229, https://doi.org/10.1038/s41598-020-64111-3, 2020.

Yang, L. H., Jacob, D. J., Colombi, N. K., Zhai, S., Bates, K. H., Shah, V., Beaudry, E., Yantosca, R. M., Lin, H.,Brewer, J. F., Chong, H., Travis, K. R., Crawford, J. H., Lamsal, L. N., Koo, J.-H., and Kim, J.: Tropospheric NO2 vertical profiles over South Korea and their relation to oxidant chemistry: implications for geostationary satellite retrievals and the observation of NO2 diurnal variation from space, Atmos. Chem. Phys., 23, 2465–2481, https://doi.org/10.5194/acp-23-2465-2023, 2023.

Zaveri, R. A., R. C. Easter, J. D. Fast, and L. K. Peters, Model for Simulating Aerosol Interactions and Chemistry (MOSAIC), J. Geophys. Res., 113, D13204, doi:10.1029/2007JD008782, 2008

Zhang, Y., Dai, J., Li, Q., Chen, T., Mu, J., Brasseur, G., Wang, T., Xue, L.: Biogenic volatile organic compounds enhance ozone production and complicate control efforts: Insights from long-term observations in Hong Kong. Atmos. Environ., 309, 119917, https://doi.org/10.1016/j.atmosenv.2023.119917, 2023.

Zhao, X., Zhou, W., and Han, L.: Human activities and urban air pollution in Chinese mega city: An insight of ozone weekend effect in Beijing, Phys Chem Earth Pt. A/B/C, 110, 109–116, https://doi.org/10.1016/j.pce.2018.11.005, 2019.

Zheng, B., Tong, D., Li, M., Liu, F., Hong, C., Geng, G., Li, H., Li, X., Peng, L., Qi, J., Yan, L., Zhang, Y., Zhao, H., Zheng, Y., He, K., and Zhang, Q.: Trends in China's anthropogenic emissions since 2010 as the consequence of clean air actions, Atmos. Chem. Phys., 18, 14095–14111, https://doi.org/10.5194/acp-18-14095-2018, 2018

Zhu, S., Ma, J., Wang, S., Sun, S., Wang, P., Zhang, H.: Shifts of formation regimes and increases of atmospheric oxidation led to ozone increase in North China Plain and Yangtze River Delta from 2016 to 2019. J. Geophys. Res.: Atmos., e2022JD038373, https://doi.org/10.1029/2022JD038373, 2023.

Table 1. Sensitivity experiments

Model Experiments	Description [a]
BASE	Without emission reduction
NOx	With emission reduction in NO_x by a factor of 2
AVOCs	With emission reduction in anthropogenic VOCs by a factor of 2
N+A	With emission reduction in NO_x and anthropogenic VOCs by a factor of 2
TOTAL	With emission reduction in all considered species by a factor of 2

[a] Relevant species in emission inputs is shown in Sect. 2.1 and Table S1 in Supplementary Materials.

Table 2. Percentage changes of surface ozone due to emission reduction in urban location

Location	Sites	Ozone changes in winter condition (Mean ± SD)			
		NOx[a]	*AVOCs*[b]	*N+A*[c]	*TOTAL*[d]
North	Beijing	25.0 ± 25.2[e]	-2.5 ± 1.3	22.0 ± 32.8	20.0 ± 19.5
East	Shanghai	33.2 ± 35.3	-18.2 ± 13.5	21.8 ± 20.5	22.7 ± 18.8
South	Guangzhou	21.4 ± 22.6	-17.1 ± 11.2	7.1 ± 3.2	10.0 ± 3.5
West	Chengdu	21.3 ± 23.8	-9.4 ± 8.5	14.1 ± 8.3	20.3 ± 13.5
Location	Sites	Ozone changes in summer condition (Mean ± SD)			
		NOx	*AVOCs*	*N+A*	*TOTAL*
North	Beijing	6.4 ± 3.8	-21.8 ± 19.2	-5.5 ± 4.2	-7.3 ± 5.0
East	Shanghai	17.1 ± 12.8	-22.9 ± 20.8	-2.9 ± 2.1	-2.6 ± 1.5
South	Guangzhou	15.0 ± 13.1	-14.5 ± 13.5	1.3 ± 1.0	1.3 ± 0.9
West	Chengdu	5.5 ± 4.5	-14.5 ± 10.2	-5.5 ± 2.0	-4.5 ± 1.9

a-d. Sensitivity cases with a 50% reduction in the emissions of NO_x (*NOx*), AVOCs (*AVOCs*), NOx and AVOCs (*N+A*), and other species (NO_x, AVOCs, CO, NH_3, SO_2) under consideration (*TOTAL*).

e. Values are displayed in the average ozone changes during daytime (06:00 to 19:00 LST) in percentage with the standard deviation as the error bar. (ozone changes= (case value – base value)/base value ×100).

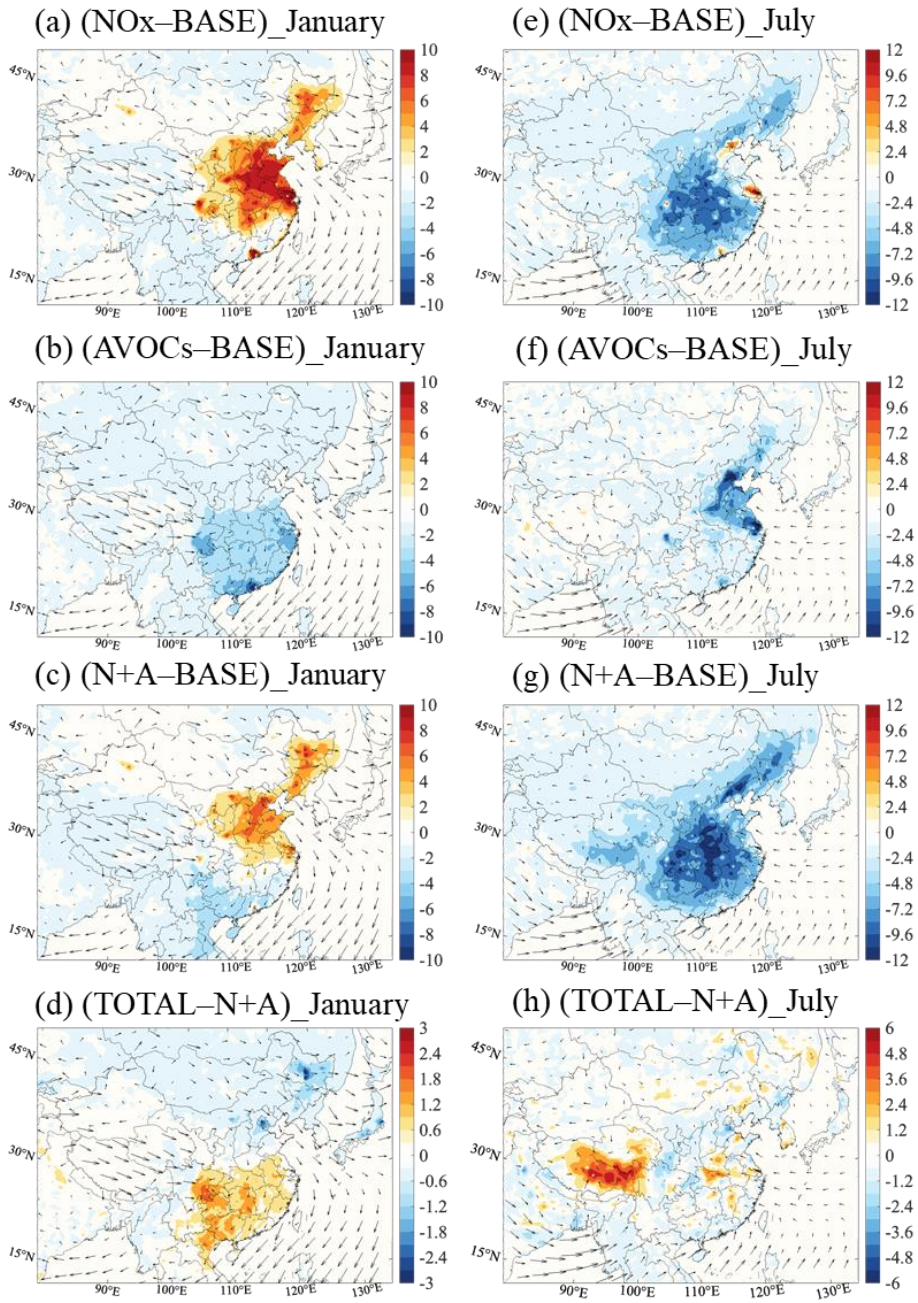

1020

Figure 1. Changes in the monthly-averaged daytime (06:00 to 19:00 LST) surface ozone concentration (Unit: ppbv) response to a 50% reduction in NO_x emissions (a, e; *NOx* case), in anthropogenic VOCs (AVOCs) emissions (b, f; *AVOCs* case) and in combined NO_x and AVOCs emissions (c, g; *N+A* case) relative to *BASE* case and to the additional reduction in the
1025 emission of CO, NH_3 and SO_2 by 50% (d, h; *TOTAL* case) relative to *N+A* case for January (a-d) and July (e-h) 2018. Arrows represent the wind speed and wind direction. Notice the inconsistency in the scale of Figure 1d and 1h.

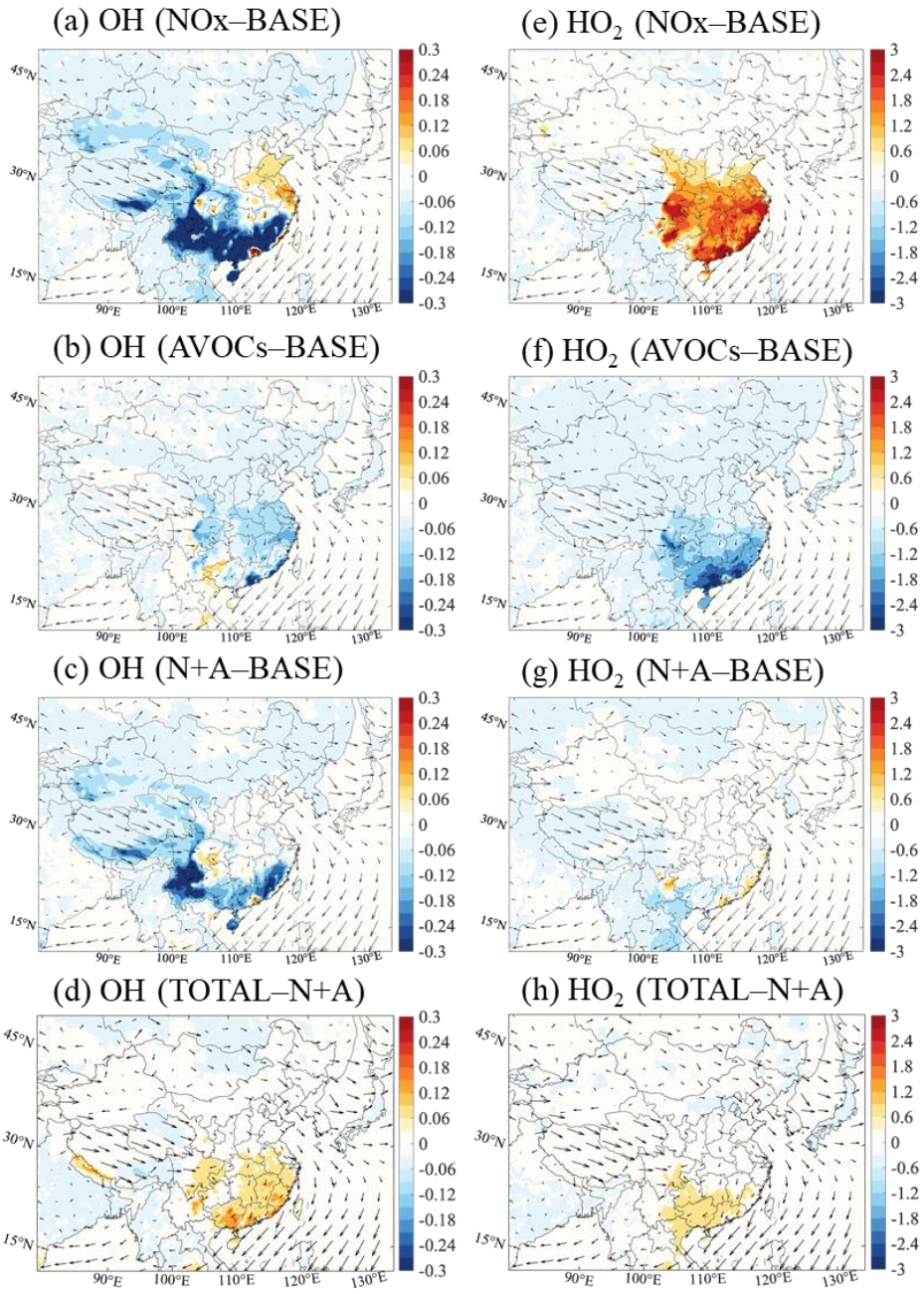

Figure 2. Changes in the monthly-averaged daytime (06:00 to 19:00 LST) surface mixing ratio of OH radical (a-d, Unit: 0.1 pptv) and HO_2 radical (e-h, Unit: pptv) response to a 50% reduction in the emissions of NO_x (a, e; *NOx* case), anthropogenic VOCs (b, f; *AVOCs* case) and in NO_x and AVOCs (c, g; *N+A* case) relative to *BASE* case and in additional emission reduction of other species (d, h; *TOTAL* case) relative to *N+A* case for January of 2018. Arrows represent the wind speed and wind direction.

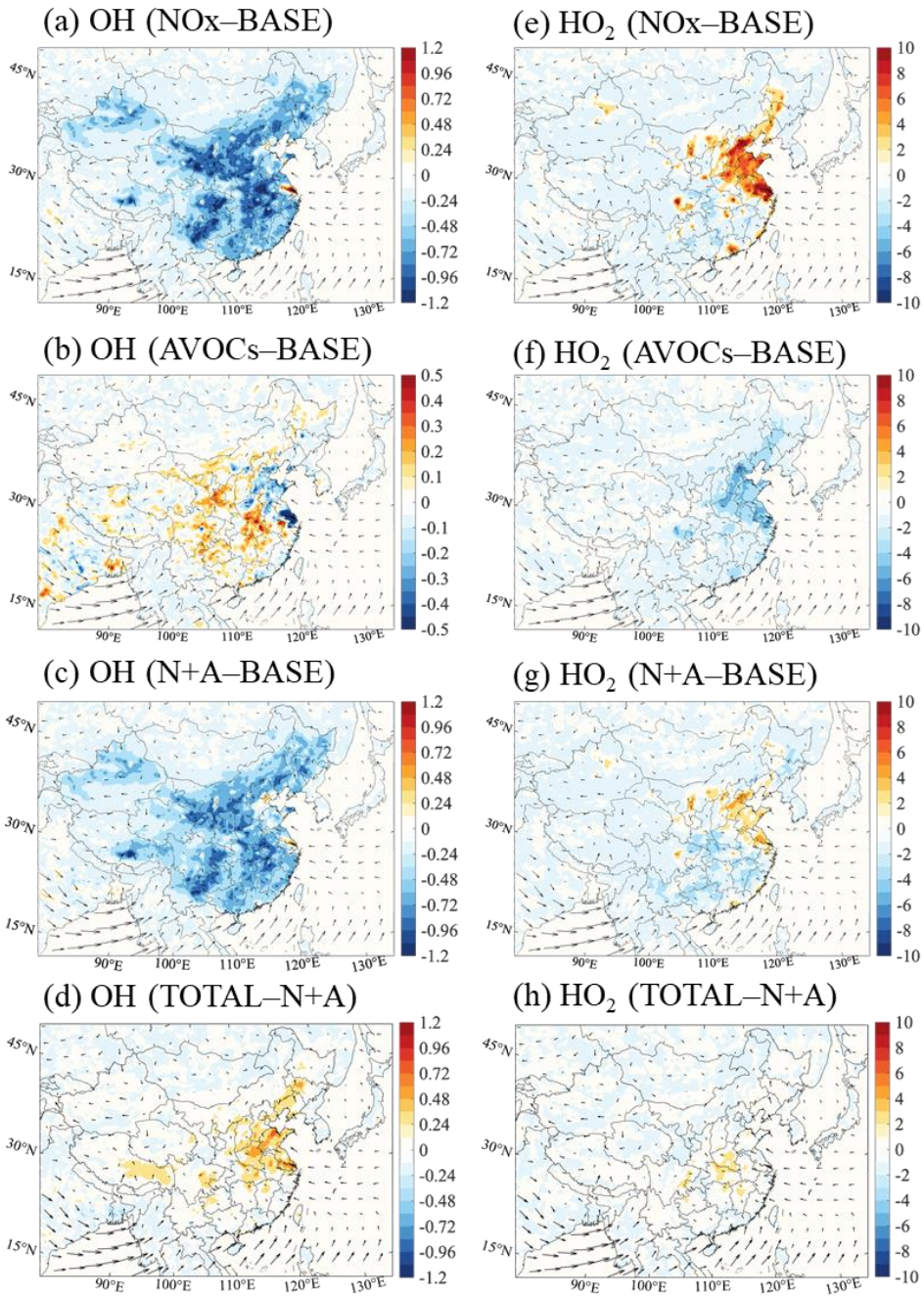

1040

Figure 3. Same as Fig.2 but for July of 2018. Notice the inconsistency in the scale of Figure 2b.

1045

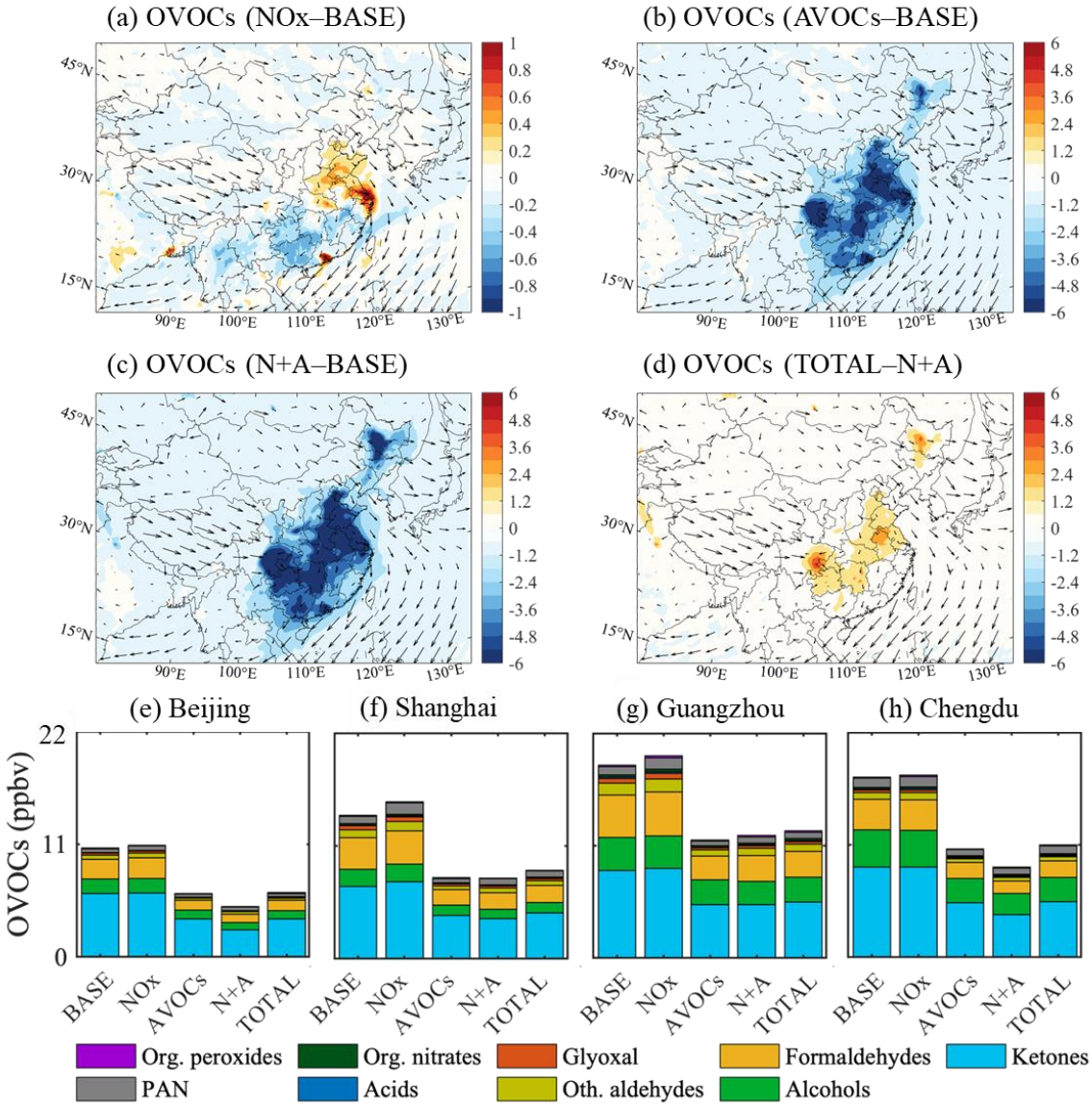

Figure 4. Changes in the monthly-averaged surface concentration of total oxidized VOCs (OVOCs) for January 2018. (a-d) Changes in the concentration of total OVOCs (Unit: ppbv) response to the reduction in the emission of NO_x (a, *NOx* case), anthropogenic VOCs (b, *AVOCs* case) and combined NO_x and AVOCs (c, *N+A* case) relative to the *BASE* case and in an additional emission reduction of other species (d, *TOTAL* case) relative to *N+A* case. (e-h) Averaged concentration of OVOCs contributed by different species at four city sites (Beijing, Shanghai, Guangzhou, and Chengdu) in China in five simulated cases (*BASE*, *NOx*, *AVOCs*, *N+A*, and *TOTAL* cases). Arrows in panel (a-d) represent the wind speed and wind direction. Notice the inconsistency in the scale of Figure 3a.

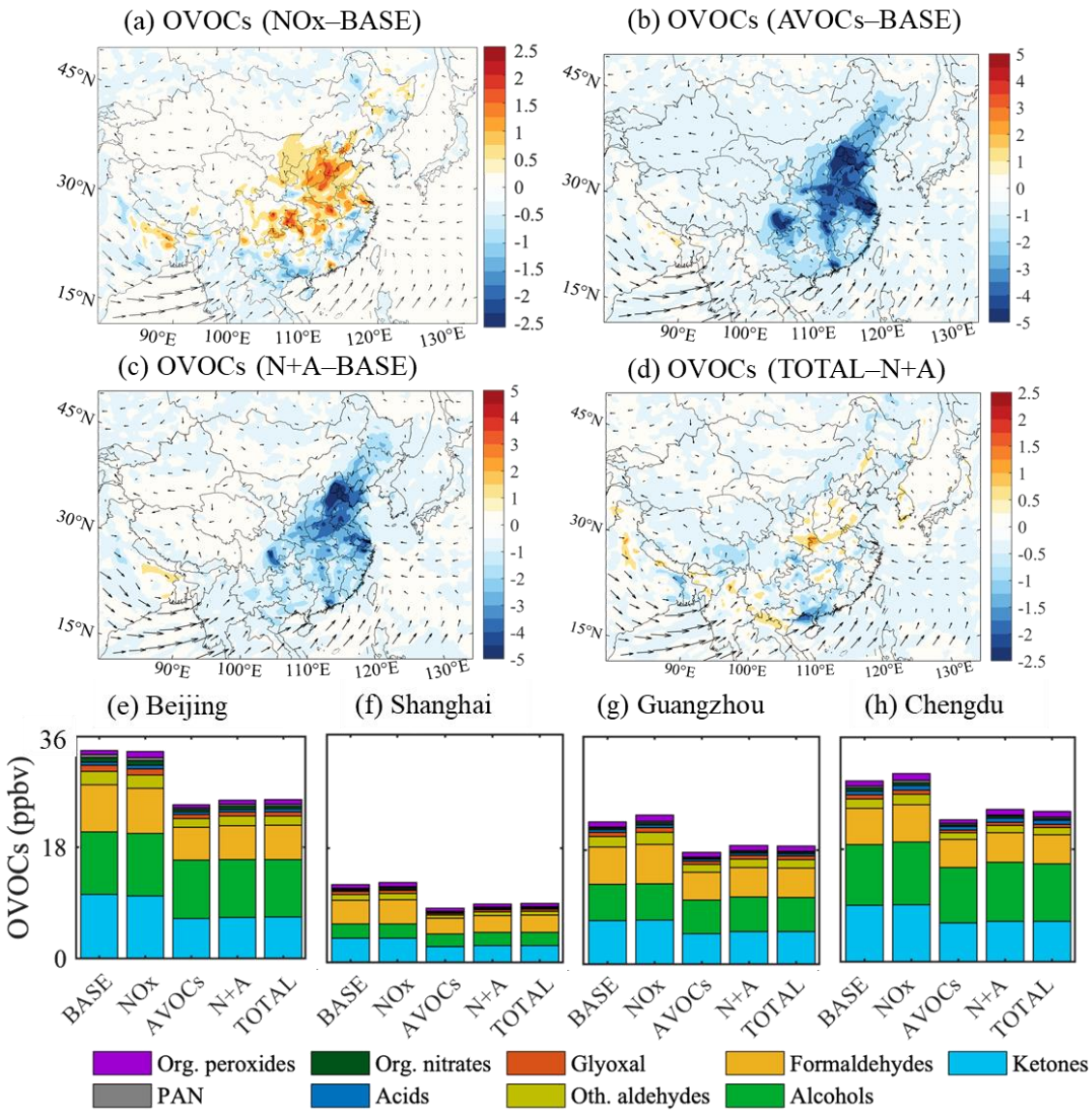

Figure 5. Same as Fig.4 but for July of 2018. Notice the inconsistency in the scale of Figure.

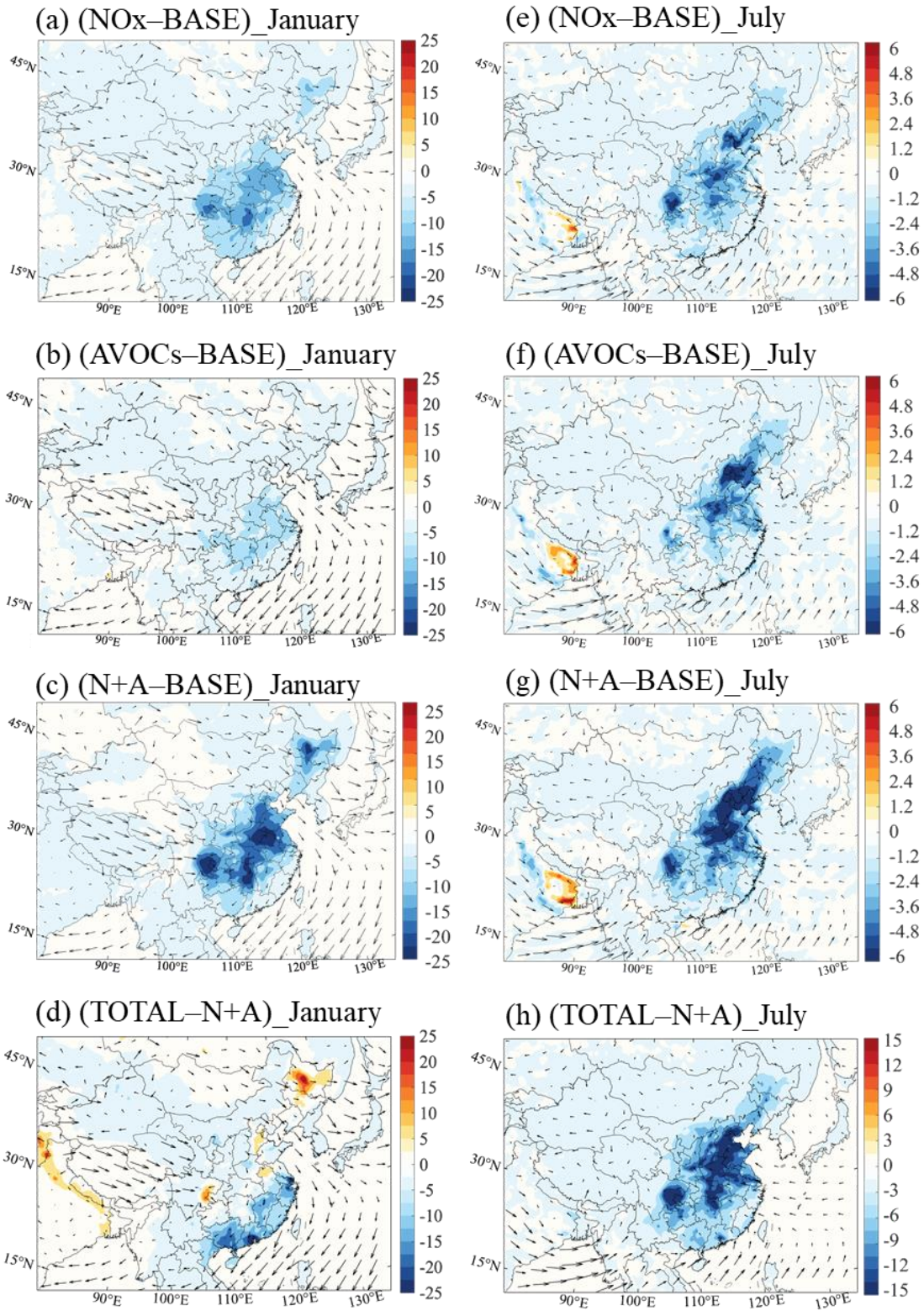

Figure 6. Changes in the monthly-averaged surface concentration of fine particulate aerosol (Unit: μg m^{-3}) in response to *NOx* (a, e), *AVOCs* (b, f) and *N+A* case (c, g) relative to *BASE* case and to *TOTAL* case (d, h) relative to *N+A* case for January (a-d) and July (e-h) 2018. Arrows represent the wind speed and wind direction. Notice the inconsistency in the cale of Figure 6h.

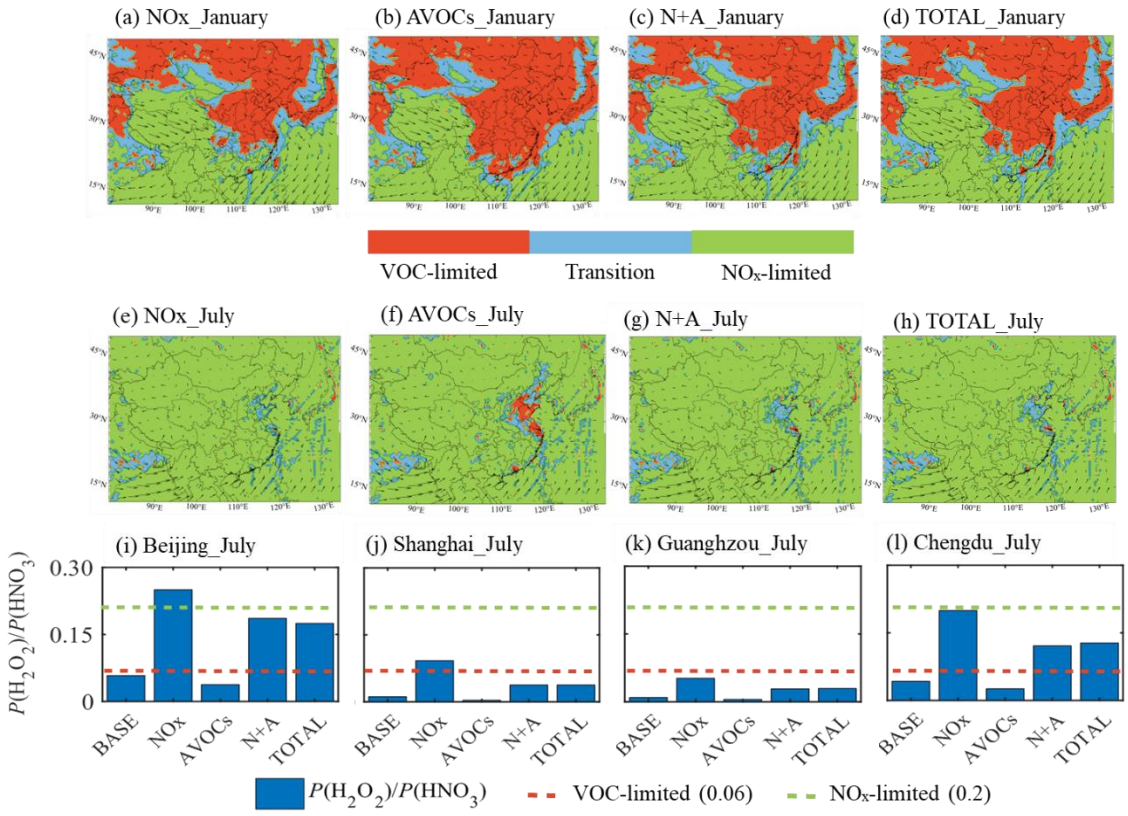

Figure 7. Impact of the emission reduction on ozone sensitivity regimes. (a-h) Display of ozone sensitivity regions in which ozone production is limited by the availability of nitrogen oxides (NO_x-limited, in green), and volatile organic components (VOC-limited, in red) under the emissions in case of *NOx*, *AVOCs*, *N+A*, and *TOTAL* conditions in January (a-d) and July (e-h) of 2018. The regions where ozone production is controlled by the availability of both NO_x and VOCs (transition) are shown in blue. (i-l) Averaged daytime (06:00 to 19:00 LST) value of the ratio between the production rate of hydrogen peroxide (H_2O_2) and nitric acid (HNO_3) [$P(H_2O_2)/P(HNO_3)$] at four city sites (Beijing, Shanghai, Chengdu, Guangzhou) in the five simulated cases (*BASE*, *NOx*, *AVOCs*, *N+A*, and *TOTAL*) for July 2018.

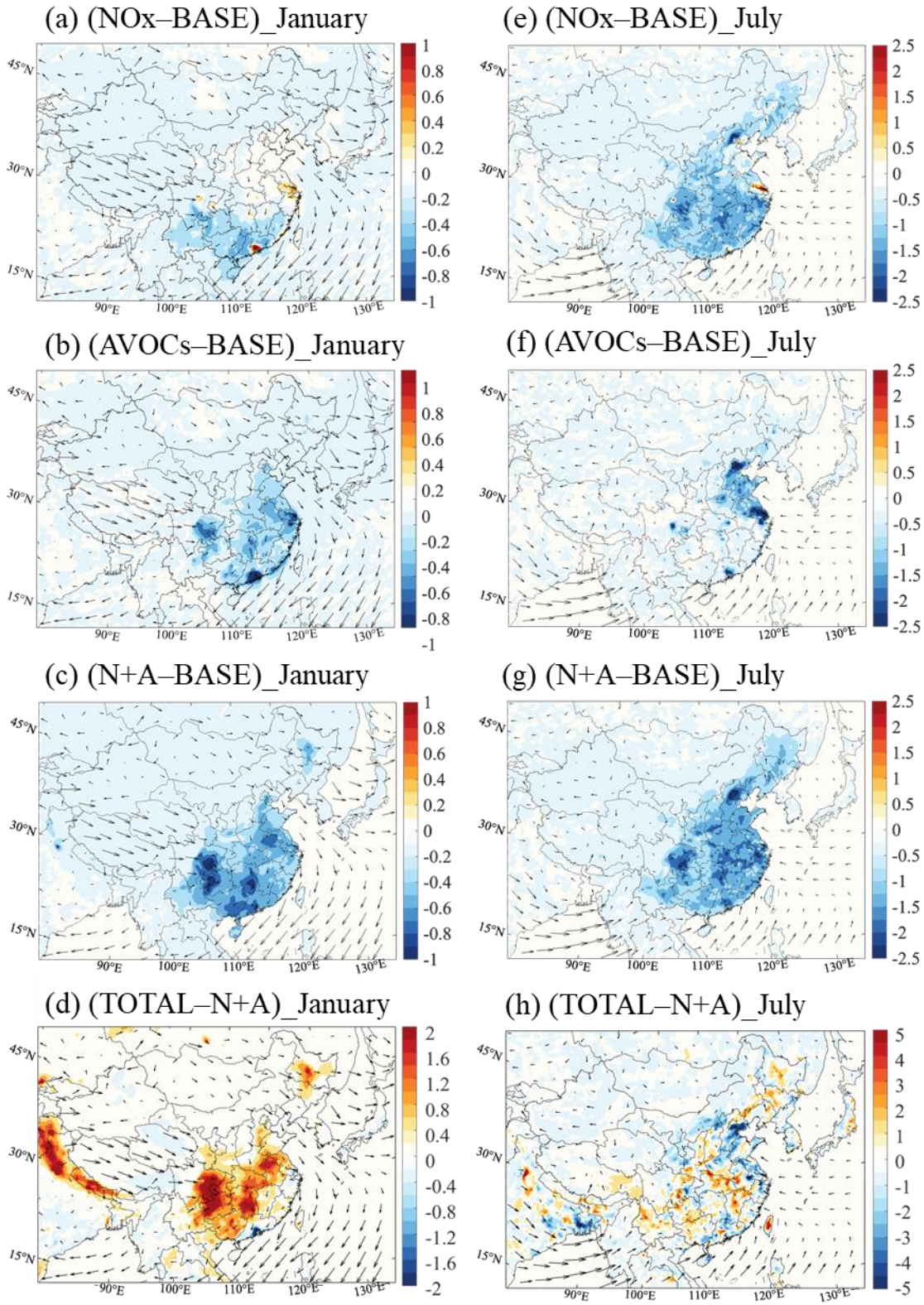

Figure 8. Changes in the monthly-averaged daytime value of atmospheric oxidizing capacity (*AOC*) response to NO_x (a, e), *AVOCs* (b, f), and *N+A* (c, g) cases relative to *BASE* case (Unit: 10^7 molec. cm^{-3} s^{-1}) and to *TOTAL* case (d, h) relative to *N+A* case (Unit: 10^6 molec. cm^{-3} s^{-1}) for January (a-d) and July (e-h) 2018.

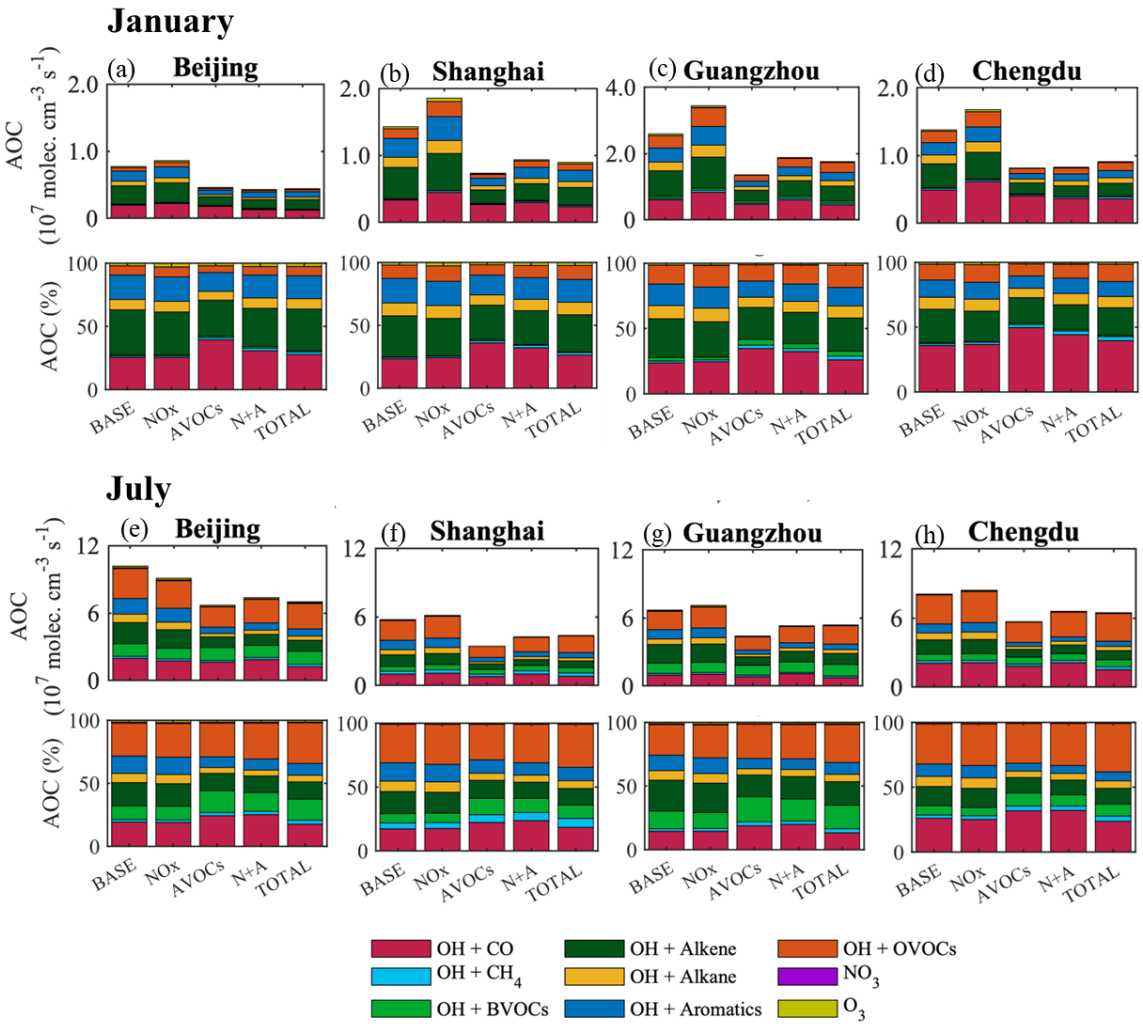

Figure 9. Monthly-averaged value (Unit: 10^7 molec. cm^{-3} s^{-1}) and relative terms (Unit: %) of daytime *AOC* at the sites of Beijing (a, e), Shanghai (b, f), Guangzhou (c, g), and Chengdu (d, h) in five simulated cases (*BASE*, *NOx*, *AVOCs*, *N+A*, *TOTAL* cases) in January (a-d) and July (e-h) of 2018. Notice the inconsistency in the scale of Figure 9c.

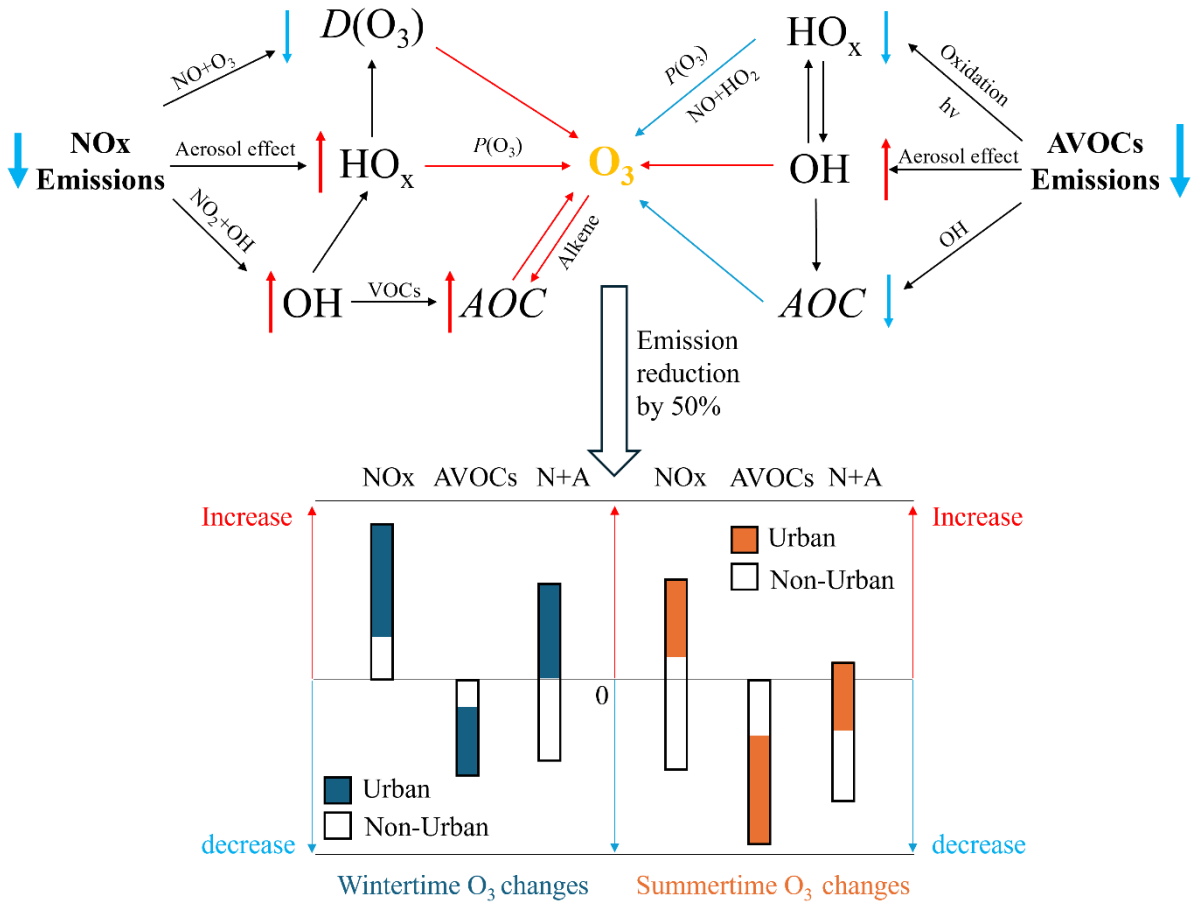

Figure 10. Schematics show the responses of oxidative processes, associated with ozone formation, to the reduction in primary emissions of NO_x and AVOCs in urban areas (VOC-limited) in winter and summer. Arrows besides the chemicals represent the changes associated with the reduction in emission. (decrease trend shown in blue; increase trend shown in red) Blue and red arrows closing to O_3 represent the positive and negative contributions to the ozone formations. *AOC*, *P*(O_3), and *D*(O_3) are the abbreviations of the Atmospheric Oxidative Capacity, production of ozone, and destruction of ozone. Bar figure shows the ranges of ozone changes in whole of China (black bar), in non-urban areas (white part in the bar), and in urban areas (colored part in the bar) in three emissions cases (*NOx*, *AVOCs*, and *N+A* represent the case with emission reduction in NO_x, Anthropogenic VOCs (AVOCs), and the combined NO_x and AVOCs emissions, respectively) relative to *BASE* cases in winter and summer conditions.